CENTRO DE INVESTIGACIONES
EN OPTICA, A.C.

“Definitive version. Includes changes suggested by reviewers”

“3D SCANNING OF OBJECTS BY DISPLACEMENT OF LIGHT LINES AND STUDY OF THEIR PROFILE”

Thesis submitted in fulfillment of the requirements for degree of Doctor of Science (Optics)

Presented by: Heyner Leoncio Vilchez Rojas

Advisor: PhD. Amalia Martínez García

Vo.Bo Advisor
March 24, 2022

León · Guanajuato · México
March 2022

In memory of my father: Leoncio Vilchez Dett.

ACKNOWLEDGMENTS

Por medio de este espacio quiero agradecer a las instituciones y personas que de alguna u otra forma han contribuido a la realización de mis estudios de doctorado y a la culminación del presente trabajo de tesis.

A la Dra. Amalia Martínez por su constante apoyo y dedicación en la asesoría de mi tesis. Al Dr. Juan A. Rayas, por sus valiosas recomendaciones en los trabajos experimentales. Gracias a ambos por brindarme sus conocimientos, experiencia académica y amistad. Espero que la vida nos dé varias oportunidades para seguir trabajando juntos.

Al comité de seguimiento de mi tesis: Dr. Manuel Servín, Dr. Francisco Cuevas y Dr. Gerardo Flores por sus comentarios e importantes sugerencias en el cumplimiento de los objetivos de este trabajo.

Al Dr. Rigoberto Juárez por asesorar mi estancia en el Centro de Investigación y Desarrollo de Tecnología Digital (CITEDI) del Instituto Politécnico Nacional (IPN). Muchas gracias Dr. Rigoberto por su interés y paciencia en mi trabajo.

A los integrantes del Grupo de Pruebas Ópticas y Mecánicas por las agradables discusiones en los distintos temas de interés científico.

Al Consejo Nacional de Ciencia y Tecnología (CONACYT) por subvencionar mis estudios en el Centro de Investigaciones en Óptica.

A mi familia. A mis padres Leoncio y Mary por su inagotable amor, apoyo y preocupación por mí. A mis hermanos Sukey y Paco por acompañarme en la distancia. Este trabajo es para ustedes y especialmente para ti padre de mi corazón que desde el cielo sigues iluminando mi camino.

Gracias a todas las personas que siempre se preocuparon por mi y ahora me acompañan desde el cielo. Tío José Rojas y Tía Maritza Domínguez, los llevo en mi corazón.

A mi esposa Liliana por su comprensión y motivación durante mis estudios. Gracias por regalarme el privilegio de ser Padre. Hijo querido, te esperamos con mucho amor.

A mis amigos del CIO por sus consejos y compañía en esta larga estadía lejos de mi familia.

Gracias Dios por cuidar de mi familia y amigos durante esta dura pandemia.

ABSTRACT

This thesis presents three different optical systems for digital tridimensional reconstruction of objects using the displacement of light lines technique. System 1: 3D scanning of objects was carried out through the projection of one light line with profiles of type Gaussian, triangular and sinusoidal. Appropriate algorithms were implemented for each type of light line profile. The efficiency of each profile was evaluated in terms of precision and processing time. System 2: 3D scanning of objects by projection of three color lines (red, green and blue) with a Gaussian profile. Color lines simultaneously scan different zones of the object with the purpose of optimizing the capture time and the number of stored images, compared to the projection of one light line. System 3: 3D scanning of objects by color structured multi-line projection with Gaussian profile was proposed. The technique consists of projecting a set of gratings with equidistant parallel lines of color red, green, and blue on the object to be reconstructed. The displacement of the color lines is obtained through image processing by skeletonization in the R, G, and B color channels. The displacements of the color lines of each grating are combined to obtain the complete shape of the object.

The results suggest the use of light projection with Gaussian profile to obtain more accuracy in the topography measurement, and the use of light with triangular profile to considerably improve the processing time and to obtain fast results. The criteria for choosing the proposals given in this thesis for scanning objects will depend on the complexity of the surface of the object and the requirements of the application, in case a high precision or speed of measurement is needed in the scanning. Illustrative examples of the obtainable experimental results are presented and discussed.

CONTENT

LIST OF FIGURES

LIST OF TABLES

INTRODUCTION

Depending on the need of the application, different scanning techniques based on the projection of structured light have been developed. Nowadays, the most popular structured light techniques are based on phase detection of a fringes pattern and in the calculation of the displacement of the light lines by extraction of the skeleton. Techniques based on phase detection include the Fourier transform profilometry (FTP) and phase-shifting profilometry (PSP), both may require complex algorithms to obtain the unwrapped phase. On the other hand, there are techniques based on the calculation of the displacement of the light lines include laser line projection (LLP) and multi-line structured light (MLSL) which require skeletonization algorithms of light lines.

The FTP is a technique simple of full-field and single-shot. This method of scanning requires only one image of the deformed fringe pattern to get the surface of the measured object, so it has an obvious advantage to obtain the dimensions of objects in real-time, so it can be applied on dynamic objects [1-5]. In this technique, it must be ensured, in the frequency space, that the fundamental component does not overlap the zero component and other higher order spectra. For this reason, that it is necessary to project a pattern of fringes with a high spatial frequency, this practice increases considerably the probability that the algorithms of phase unwrapped will fail. In general, this technique fails when measurements of complex surface geometry are made or if there are abrupt geometric discontinuities in the scene.

The PSP technique is also full-field that can obtain the 3D shape of objects with a higher resolution than the FTP technique [6-11]. However, this technique has limited applications in measuring the shapes of moving objects or deformable objects because it requires the processing of a minimum of three images. A new source of error is introduced if the phase step is carried out by a piezoelectric due to the non-linear response of this device [12, 13]; however, this phase step error is negligible by using a multimedia projector. Like the FTP technique, it is necessary to implement complex algorithms of phase unwrapping which are susceptible to failure if the height variations of the object are abrupt.

The LLP technique scans objects through of displacement (or deformation) that suffers the projected line on the surface of the object [14-16]. Its application is limited to

static objects only. The main advantage of this technique is that it is not necessary to implement complex algorithms of phase unwrapping, there is no problem of ambiguity of the line, it is highly robust when processing images of lines with large discontinuities, and has a greater ability to obtain 3D shapes of objects with complex surfaces. Therefore, this technique can solve the limitations of the FTP and PSP techniques, when it is desired to get the 3D shape of static objects; however, the paid price is the storage and processing of a large number of images, and consequently a larger processing time. Regarding the mechanical implementation, the LLP technique requires linear translation systems to move the light line onto the entire surface of the object, a cylindrical lens to extend the laser light in a continuous line, and some cases it is necessary to mount a filter on the camera lens to eliminate ambient light and improve the signal-to-noise ratio [17]. These elements hinder the mechanical implementation of the technique in industrial environments [18-20]. Regarding the projected light, this cannot easily modify its characteristics such as intensity, width, and profile because this is limited by the laser properties and the cylindrical lens. Additionally, the speckle pattern generated by the laser is one of the most important factors that deteriorate the images of the light line and consequently on the measurements of the object dimensions [18, 21-24]. There are robust techniques to reduce the speckle pattern noise in the images of the light lines; however, their implementation requires digital filters and a greater number of computational operations, which reduces the performance of the technique in terms of processing time [22, 24].

The MLSL technique scans objects by projection of multi-line structured light [25-30]. Although it does not need complex phase unwrapping algorithms either, and can get the 3D shape of moving objects or deformable objects; however, its main limitation is its low resolution [25, 31]. Some authors use interpolation methods to increase the resolution of the technique; obviously, these methods fail if the object has a high texture on its surface. When trying to increase the number of projected lines in order to increase resolution, the problem of indexing of the lines must be solved [27-29, 32] otherwise it will be impossible to obtain the 3D shape of the object. It is possible to use a laser light source to generate the multi-lines of light [31, 33, 34]; however, the implementation of the optical system loses simplicity regarding the use of the multimedia projector. On the other hand, there are to deal with the noise of the speckle pattern generated by the laser, which is one of the most important factors that directly affect the measurements of the

object dimensions. Due to this technique works by the grouping of the distorted lines, the grouping algorithms fail large discontinuities caused by abrupt variations in the object height. In addition, the color of the surface reduces the effectiveness of the segmentation of the light lines. The use of this technique is only limited to the reconstruction of objects with smooth surface, with some symmetry, and that do not have contrasting colors.

All optical techniques with structured light projection are promising but not perfect. The criteria to judge whether an optical technique is good depends specifically on the application. In this thesis, we present the results of three proposals for the 3D digitization of objects through the projection of structured light.

We propose the projection of white light profiles for scanning objects. Our proposal includes the projection of three types of light profiles (Gaussian, triangular and sinusoidal), as well as the algorithms necessary to obtain the 3D shape with each of them. We analyze each light profile with its respective algorithm in terms of accuracy and processing time for the reconstruction of a test object. We use a multimedia projector as a light source, instead of a laser light source, which allows to project a line of white light generated digitally. The projected light line is move in steps of one pixel across the entire surface of the object, and whose step length will depend on the resolution of the multimedia projector. In addition, since the light line is generated digitally, the width, intensity, and profile of the light can be easily varied and not be limited only to the Gaussian profile of the laser light. Using the multimedia projector will facilitate the mechanical implementation of the optical system because the linear translation system is dispensed with. The main advantage of using the multimedia projector is that the projected light is free of speckle pattern noise which is the most important cause in the loss of accuracy of the LLP technique [21, 23, 24].

Also, we will extend the study of our previous work [16], where we used a white light line with different profiles to optimize accuracy and processing time for the reconstruction of the 3D shape. We propose the 3D scanning of objects using the simultaneous projection of three color lines (red, green, and blue) with Gaussian profile. These lines scan spatially different zones of the test object simultaneously with the purpose of optimizing the capture time and the number of stored images, compared to projection one light line. To carry out our proposal, we will take advantage of the RGB color channels of the CCD camera and segment each color line with its respective color

channel. In this way, each line will be able to independently reconstruct, in each color channel, different zones of the object simultaneously, then these reconstructed zones will be assembled to obtain the complete 3D shape of the object. Furthermore, since the projected lines are of the Gaussian type, we will carry out the skeletonization process of the projected lines by implementing the Bezier polynomial method combined with the bisection method. These skeletonization methods allow to obtain better results of the 3D reconstruction in terms of precision and processing time [14, 16]. Although this proposal is limited to the application of static objects, it allows us to reconstruct objects with high pixel density and also lacks the ambiguity problem, which allows scanning objects with large measuring depths.

Finally, we propose obtaining the 3D shape of objects through scanning by color structured multi-line projection with Gaussian profile. The 3D shape is obtained by measuring the displacements of each light line caused by a test object. Processing of images is carried out in each color channel R, G, and B, and aims to recognize light lines through the processes of segmentation, grouping and skeletonization that we propose. Regarding segmentation, we propose filter the images in the frequency space by designing a Butterworth filter, and then carry out the binarization procedure by thresholding [35]. To reduce the number of broken fringes, we propose the use of the morphological operation of dilation [36] on the images. In respect of grouping and skeletonization, both procedures are carried out iteratively one after the other for each line and on each color channel. We propose a simple algorithm based on the areas of the line segments of the captured images. Detecting the line segments that belong to one line allows us to group them and later obtain the skeleton positions of the line in question. The displacements of the lines skeleton that scan an object are obtained with respect to a reference plane. By means of the displacements, the three-dimensional measurements of objects are obtained previous calibration process which is based on reference [10]. The results show that the object is reconstructed with a high resolution, and the proposal has the merit of capturing images in a significantly faster time compared to the technique of projection of one light line.

It is important to highlight that the innovative use of different methods based on structured light projection proposed in this thesis will allow expanding the range of possibilities in obtaining the 3D shape of objects. The criteria for choosing the different techniques of suitable structured light projection will depend on the application

requirements, either high accuracy of measurement or speed of it. It is important to highlight that this technique has a wide range of applications such as the digitization of cultural heritage, medicine and industry [20, 21, 37-42].

OBJETIVES

General Objective

To measure the 3D surface shape of objects by skeletonizing lines projected by a digital projector.

Specific Objectives

- To scan objects in 3D by projecting a line of white light by using Gaussian, triangular and sinusoidal profiles.
- To implement the appropriate algorithms to get the skeleton of the lines with sub-pixel accuracy for each type of profile.
- To evaluate the performance of each projected light profile in terms of accuracy and processing time.
- To obtain the 3D shape of an object by simultaneous scanning of three color lines (red, green, and blue).
- To implement 3D scanning of objects by the projection of multiple structured lines in color.

THESIS CONTENTS

This thesis is organized in six chapters. Chapter 1 gives a general description of the best known optical techniques for 3D scanning objects by structured light projection, which are based on the detection of the phase of a sinusoidal fringes pattern, and on the direct calculation of the displacement of the projected light lines. Chapter 2 describes the algorithms to measure the displacement of the light lines, previously applying skeletonization processes based on the Bezier curves, linear regression and non-linear regression methods. Chapter 3 describes the experimental development of 3D object scanning by projecting one light line with Gaussian, triangular and sinusoidal profiles,

respectively. The efficiency of the use of light profiles in 3D scanning is evaluated in terms of accuracy and processing time. Chapter 4 extends the study of the previous chapter where we propose 3D scanning by projection of three color lines with Gaussian profile. The segmentation by color of the projected lines is described and the efficiency of the algorithms on objects that have a colored surface is shown. Chapter 5 describes 3D scanning of objects by color structured multi-line projection with Gaussian profile. The processes of segmentation by color, the grouping and skeletonization of the projected lines in each color channel are detailed. In addition, the calibration process to obtain the dimensions of the object in units of length is described. Finally, chapter 6 mentions the general conclusions and future works of this thesis.

CHAPTER 1: 3D SCANNING TECHNIQUES OF OBJECTS BY PROJECTION OF STRUCTURED LIGHT

In this chapter, basic concepts on the optical techniques of 3D scanning of objects by structured light projection are described. The first part describes the 3D scanning technique based on detecting the phase of a cosine fringes pattern projected on the surface of an object. The relationship between the phase of the fringe pattern and the height of the object is shown. The FTP and PSP techniques, that allow obtaining the phase, are concisely described. In the second part, the 3D scanning technique based on the displacement of the line by extraction of the skeleton is described in a general way. The technique of projection of one laser light line (LLP) and the technique of projection of multi-line structured light (MLSL) are described. The relation between the displacement of the light lines and the height of the object is shown. Since the description of skeletonization algorithms are extensive and are the basis of this thesis work, the details of these algorithms will be treated in the next chapter.

1.1 TECHNIQUE BASED ON PHASE DETECTION

The technique consists of generating a sinusoidal fringe pattern and projecting it onto an object to be reconstructed. The scheme of a typical fringes projection system is shown in Fig. 1.1.(a) which consists of a projector, a camera, and a computer. The projector illuminates the objects with pre-designed fringes patterns, the camera captures the distorted fringes patterns due to the surface of the object, and the computer synchronizes both devices and performs image processing.

According to Fig. 1.1.(b), which represents in a simple way the parallel-optical-axes geometry proposed by Takeda and Kazuhiro [1], assuming a telecentric system, a fringe pattern is projected normal to the plane of the figure. The conjugate image (with period p) is formed by the projector lens on the reference plane. The camera and projector are located at the same distance D from the reference plane. Due to the presence of the object, the fringe located at point A on the reference plane impinges in point P on the object. Therefore, the fringe in question, has been displaced from A to B on the reference plane; this displacement is represented by $s(x, y)$. It is important to mention that depending on the height $h(x, y)$ of the object, different displacements will occur for each point of the fringe pattern projected on the object, which are visually manifested as a distortion in the fringes.

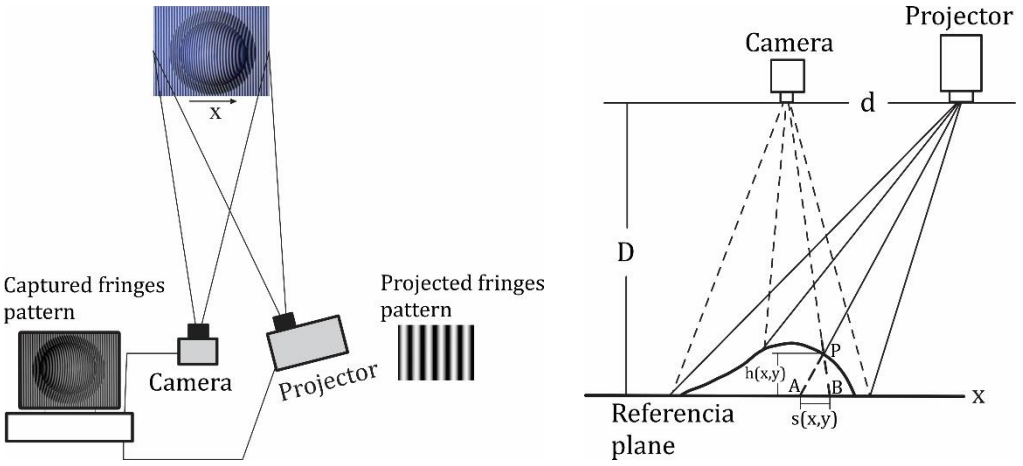

(a) (b)

Figure 1.1. (a) Typical fringe projection system. **(b)** Geometrical explanation for a point on the surface.

When the fringes are projected on the reference plane ($h(x,y) = 0$), the image of the projected fringe pattern is observed by the camera as a regular fringe pattern, which can be expressed by:

$$I_0(x,y) = a(x,y) + b(x,y)\cos\left[\frac{2\pi}{p}x\right] \qquad (1.1)$$

where (x,y) denotes the points of the fringes pattern, $a(x,y)$ is the background light, $b(x,y)$ is the intensity modulation and p is the period of the fringe pattern.

For an object with height variations $h(x,y)$ placed on the reference plane, the phase of the deformed fringe pattern varies based on the displacement $s(x,y)$; now the captured image is mathematically defined as:

$$I(x,y) = a(x,y) + b(x,y)\cos\left[\frac{2\pi}{p}(x + s(x,y))\right]$$

$$I(x,y) = a(x,y) + b(x,y)\cos\left[\frac{2\pi}{p}x + \frac{2\pi}{p}s(x,y)\right] \quad (1.2)$$

or

$$I(x,y) = a(x,y) + b(x,y)\cos\left[\frac{2\pi}{p}x + \emptyset(x,y)\right] \quad (1.3)$$

where $\emptyset(x,y)$ is the phase modulation resulting from the object height distribution $h(x,y)$. From Eqs. (1.2) and (1.3) the following expression is obtained:

$$s(x,y) = \frac{p}{2\pi}\emptyset(x,y) \quad (1.4)$$

Furthermore, according to Fig. 1.1.(b), by triangulation it is obtained:

$$h(x,y) = \frac{Ds(x,y)}{d + s(x,y)} \quad (1.5)$$

Finally, replacing Eq. (1.4) in Eq. (1.5), we obtain:

$$h(x,y) = \frac{Dp\emptyset(x,y)}{2\pi d + p\emptyset(x,y)} \quad (1.6)$$

Using Eq. (1.6) it is possible to obtain the height distribution of the object by calculating the phase distribution of the fringe pattern projected on the object. Although there are currently different techniques for phase extraction, the most widely used are the FTP technique [1-5] and PSP technique [6-11].

The FTP technique allows to obtain the shape of objects with a single image, so it can be applied to the scanning of moving objects. This method consists of expressing the intensity distribution of the fringes of the Eq. (1.3) to the complex form using the relation $c(x,y) = (1/2)b(x,y)exp[i\emptyset(x,y)]$ as:

$$I(x,y) = a(x,y) + c(x,y)exp(2\pi i f_0 x) + c^*(x,y)exp(-2\pi i f_0 x) \quad (1.7)$$

where c^* represents a complex conjugate of c, and $f_0 = 1/p$ is the spatial frequency of the fringe pattern (or carrier frequency). If the one-dimensional Fourier transform is performed in terms of the x-coordinate of Eq. (1.7), the spatial frequency spectrum along the axis is derived as:

$$FT[I(x,y)] = A(x,y) + C(f - f_0, y) + C^*(f + f_0, y) \quad (1.8)$$

where the capital letters denote the Fourier spectra and f is the spatial frequency in the x-direction.

According to Fig. 1.2, if we select the carrier frequency f_0 sufficiently greater than that of the spatial variations of $a(x,y)$ and $b(x,y)$, the principal spectra A, C and C^* can be easily separated. By applying sequential processing, which consists of the extraction of the component $C(f - f_0, y)$ with a window filter, its spectrum shift to the zero frequency position, and the inverse of the Fourier transform of the modified signal, the components of the carrier frequency f_0 are removed and only the desired component $c(x,y)$ is demodulated [43]. The wrapped phase distribution $\emptyset(x,y)$ can be calculated by the arctangential relationship for the real and imaginary parts of $c(x,y)$:

$$\emptyset^w(x,y) = tan^{-1}\frac{Im[c(x,y)]}{Re[c(x,y)]} \quad (1.9)$$

where the superscript w in $\emptyset^w(x,y)$ emphasizes that the values of phase are given in the interval (-π, π] rad due to the periodicity of the trigonometric functions. The calculation of the function $\emptyset(x,y)$ from its wrapped values $\emptyset^w(x,y)$ is a process known as phase unwrapping, denoted by:

$$\emptyset(x,y) = \mathcal{W}^{-1}[\emptyset^w(x,y)] \quad (1.10)$$

where $\mathcal{W}$ is the wrapping operator. Several useful phase-unwrapping algorithms have been reported [44-46] to get the phase $\emptyset^w(x,y)$ of module 2π.

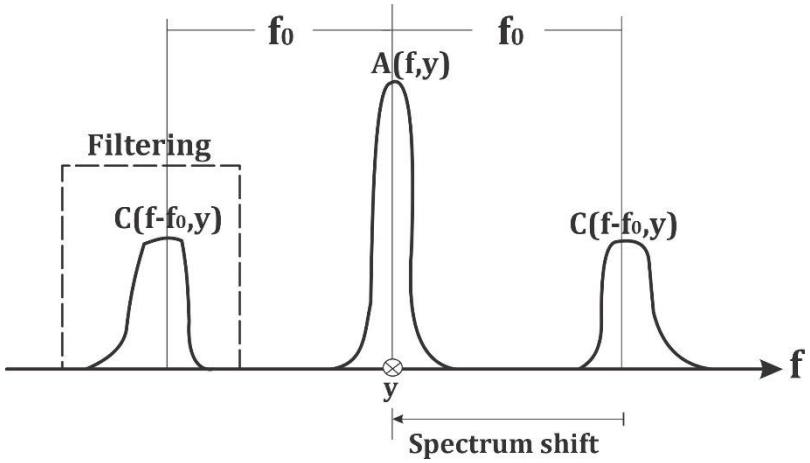

Figure 1.2. Filtering and shift in spectrum space.

On the other hand, another of the methods usually used to obtain the phase $\emptyset(x,y)$ is the phase-shifting method by N-step. From Eq. (1.3), the mathematical representation of the sequential projection of a fringe pattern onto the surface of an object is denoted as [6]:

$$I_n(x,y) = a(x,y) + b(x,y)\cos\left[\Phi(x,y) + \delta_n\right] \tag{1.11}$$

where $\Phi(x,y) = 2\pi f_0 x + \emptyset(x,y)$, and δ_n is an additional phase term known as phase shift which is given by:

$$\delta_n = \frac{2\pi(n-1)}{N}, \quad n = 1, 2, \dots, N \tag{1.12}$$

The function of wrapped phase $\Phi^w(x,y)$ can be recovered from the following equation:

$$\Phi^w(x,y) = tan^{-1}\left[\frac{\sum_{n=1}^{N} I_n(x,y)\sin\delta_n}{\sum_{n=1}^{N} I_n(x,y)\cos\delta_n}\right] \tag{1.13}$$

Applying the phase unwrapping algorithms on the function $\Phi^w(x,y)$, it is possible to calculate the function $\Phi(x,y)$ which contains the information of $\emptyset(x,y)$.

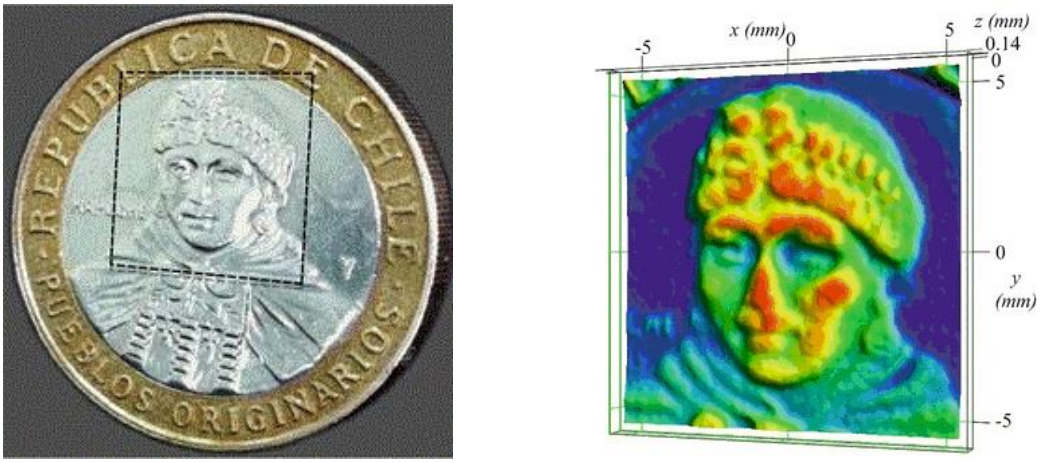

(a) (b)

Figure 1.3. (a) Object to be reconstructed by the FTP method (Chilean coin). **(b)** Object reconstructed by the FTP method [48].

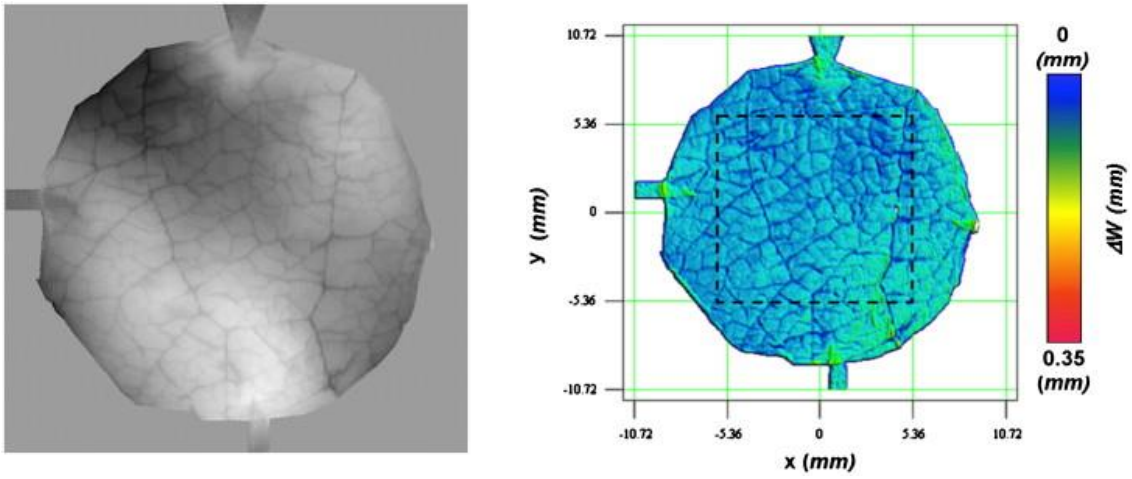

(a) (b)

Figure 1.4. (a) Object to be reconstructed by the PSP method (leaf cuticle of deciduous Apple tree). **(b)** Object reconstructed by the PSP method [49].

The appropriate choice of phase extraction method depends on the situation, e.g., if reconstruction of dynamic (or deformable) objects is required, the FTP technique is more appropriate, because it only requires one image. If not, the PSP technique should be preferred for its higher spatial resolution. In Fig. 1.3 and Fig. 1.4 the obtaining of the 3D shape of objects is observed by means of the FTP and PSP technique [47, 48], the resolution in both techniques is evident.

Although the principle of scanning by projection of fringes is simple, in practice some considerations must be taken into account since they limit the implementation of this technique due to the fact that they introduce important sources of error. On many occasions, it is not possible to avoid noise in the images (for example, in industrial applications), and depending on the shape of the object it is usual that the captured fringes present long discontinuities, which leads to a reduction in the efficiency of the phase unwrapping algorithms and it is possible that they fail. Currently, the unwrapping of the phase is one of the most challenging and important problems of this technique. On the other hand, the non-linearity of the projector and the camera [49-52], and the divergence of the light do not allow to obtain having a fringe pattern with a constant period which results in a phase error and [53, 54], therefore, a measurement error. For this reason, some investigators avoid calculating the topography by phase unwrapping and prefer to directly locate the positions of the fringes [55, 56]. The aforementioned are some important considerations that in some applications cannot be corrected and consequently the scanning of the object cannot be carried out.

1.2 TECHNIQUES BASED ON THE DISPLACEMENT OF THE LIGHT LINE

The technique of projection of one laser light line (LLP) allows obtaining the 3D shape with high resolution and pixel density of static objects, translating the line of light over the entire surface of the object. The most important advantages of this technique are that it is not necessary to implement complex phase unwrapping algorithms, it is robust to non- linearity of the devices, there is no problem of ambiguity of the line [28, 57], it can deal with large discontinuities, has a great ability to obtain 3D shapes of objects with

complex surfaces; although the paid price is the storage and processing of a large number of images.

The scheme of a typical light line projection system is shown in Fig. 1.5.(a) which consists of a light line source (it can be a laser or multimedia projector), a camera, and a computer. This technique projects a light line onto the surface of an object. The line suffers displacements in the perpendicular direction. A camera placed with an appropriate position and orientation observes the displacements of the light line from the surface. The object height data are obtained from these displacements. The displacements of a light line are measured by extracting the skeleton from its image through determining the position of the maximum intensity value in each column (or row, depending on the light line orientation), along the horizontal light line [16, 58-62].

In Fig. 1.5.(b), the geometric scheme of the optical system is shown. The distances between the optical elements (multimedia projector and CCD camera) and the reference plane are shown in said figure, the reference plane is located on the $x - y$ plane, and the data of the object heights regarding the reference plane are represented by $h(x, y)$. When a ray of the light line is projected onto the object at point P, the ray onto the reference plane is displaced from A to B. In the same way, this displacement occurs at all points where the line of light was projected and is represented by $s(x, y)$. If the distances D and d are known, and the displacements $s(x, y)$ are calculated in real units, then the height of the object along the light line is obtained by triangulation, using Eq. (1.5).

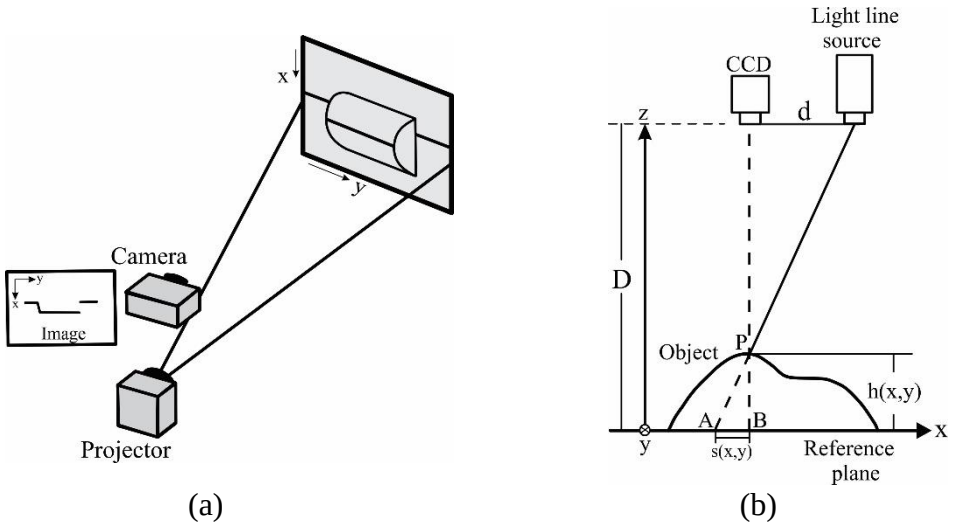

(a) (b)

Figure 1.5. (a) Typical projection system of one light line. **(b)** Geometry of the experimental arrangement of the scanning system by projection of a line of light.

On the other hand, it is also possible to obtain the 3D shape of objects by the projection of multi-line structured light (MLSL) whose light source could be generated by a multimedia projector or a laser source [26, 31, 34]. This technique is single shot; however, its main limitation is the low lateral resolution. For example, according to references [25, 26], the authors use a camera (Grasshopper3 GS3-U3-15S5C) which has a resolution of 1384x1032 pixels, to capture an image of the object with 60 horizontally projected lines of light, wasting 972 horizontal pixels, which is equivalent to approximately 94% of the image area of which information is unknown. Therefore, in the best case, only 6% of the 3D surface of the object can be reconstructed. Although the authors use interpolation methods to increase the resolution of the technique, these methods will inevitably fail if the object has a high texture on its surface. According to Fig. 1.6, for a telecentric geometry, the number of projected lines (L) is limited by the following expression [27, 28]:

$$L \leq \frac{\triangle x}{\triangle h \,.\tan(\theta)} \qquad (1.24)$$

where θ is the triangulation angle and $\triangle x$ is the lateral width of the measurement field, and $\triangle h$ is the measurement depth. According to Eq. (1.14), it is possible to increase the projected lines, but the object height to be measured should be reduced; otherwise, you will have to deal with the problem of ambiguous line indexing, which makes the shape of

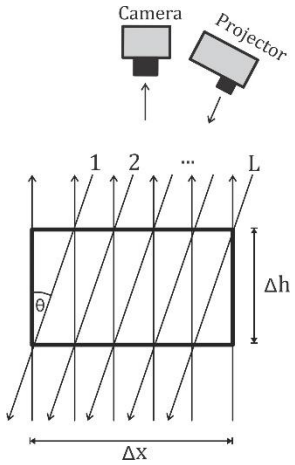

Figure 1.6. The achievable number of lines L depends on the triangulation angle θ and the unique measurement depth $\triangle h$.

the object impossible to obtain. The only way to solve this problem is placing additional cameras to the optical system [27, 28].

Due to this technique works by the grouping of the distorted lines, it is very susceptible to failure when there are occlusions or large discontinuities caused by shadows or abrupt variations in the object height [25, 26, 63]. The grouping methods are specifically designed for different object shapes in specific positions, but when the object or its position is changed, the grouping methods inevitably fail again in most cases, and these have to be significantly modified. Therefore, even though the technique is single-shot, this capacity may not really be exploited when you want to reconstruct dynamic objects.

Finally, either for the LLP or MLSL technique, the calculation of the displacements of the light lines produced by the object with respect to a reference plane is carried out by processing the captured images. The objective is to obtain the skeleton of the light line by adjusting the intensity distribution of the pixels to a continuous function. This process makes it possible to obtain the positions of the skeleton of the light lines with sub-pixel accuracy. The displacements $s(x, y)$ between the skeleton image of the light lines projected on an object, regarding the skeleton image of the same light lines projected on a reference plane is calculated, in a practical way, by the difference between both images. Since the displacements are calculated in units of pixels, it will be necessary to convert them to real units by determining the size of each pixel. The data obtained from the displacements of each skeleton are stored into an array memory what allows to obtain the complete surface shape of the object.

In Fig. 1.7 a dental piece is shown and its reconstruction using the LLP technique [21], is evidenced a high lateral resolution. In Fig. 1.8, the reconstruction of an object by the MLSL method is shown [31] where the very low lateral resolution is evident so it was necessary to use interpolation methods.

Currently, in the literature there are several algorithms to extract the skeleton of the light line with sub-pixel accuracy. The vast majority of algorithms for calculating the skeleton are based on the Gaussian profile of the laser light line. However, in this thesis work is proposed to generate the light lines by using a multimedia projector which allows modifying the profile of the projected lines and generating the appropriate algorithms for each type of profile. These algorithms are based on the Bezier curve method, linear

regression and nonlinear regression, depending on the projected light profile. The use of the light profile will depend on the application in case a shorter processing time or higher precision is required. Since the description of this algorithms are extensive, the details will be treated in the next chapter.

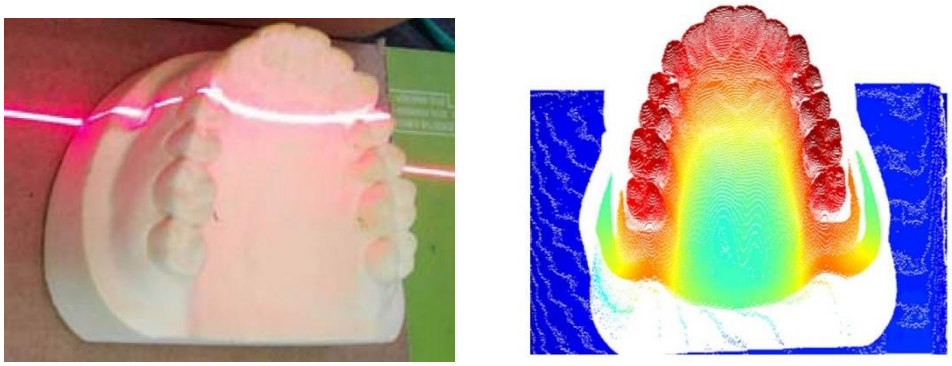

(a) (b)

Figure 1.7. (a) Object to be reconstructed by the LLP method. **(b)** Object reconstructed by the LLP method where a high density of pixels is observed in the reconstruction [21].

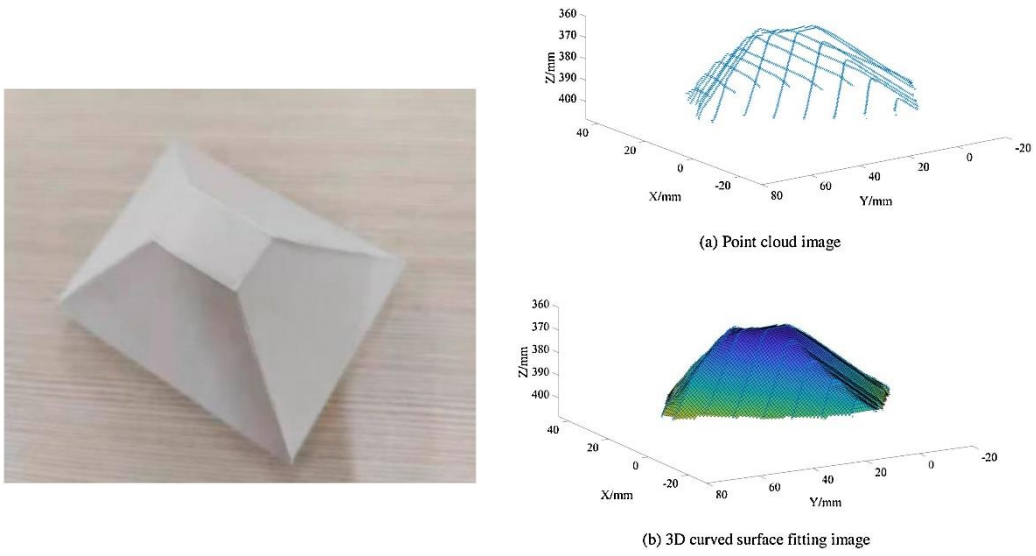

(a) (b)

Figure 1.8. (a) Object to be reconstructed by the MLSL method. **(b)** Object reconstructed by the MLSL method. In the upper part, the reconstructed object is observed with very low resolution and in the lower part, the surface is shown the object which has been interpolated [31].

1.3 CONCLUSIONS

In this chapter the basic concepts of the techniques of 3D scanning of objects by structured light projection using the phase detection techniques of a fringe pattern and the detection technique of the movement of light lines were described.

In the phase detection technique, the Fourier Transform profilometry (FTP) and the phase-shifting profilometry (PSP) were presented. The scanning principle of both methods is simple, however, in practice, important considerations must be taken into account which introduce critical errors in the calculation of the phase, and consequently in the measurement of the dimensions of the object. Some results reported in the bibliography were shown.

On the other hand, with respect to the technique of displacement of one laser light line (LLP), the method of projection of one light line is robust to long discontinuities, however, its main disadvantage is the storage and processing of a large number of images. The projection method of multi-line structured light (MLSL) can obtain the shape of the object by a single image; however, its main disadvantage is the low resolution. Some results reported in the bibliography were shown.

The description made in this chapter will allow the comparison of the proposal of our work, with respect to other 3D object scanning techniques.

CHAPTER 2: ALGORITHMS TO DETECT THE POSITION OF A LIGHT LINE IN AN IMAGE

A multimedia projector allows digitally generate different profiles of light and projects them onto the surface of some object; therefore, to obtain the skeleton of the light line it is necessary to implement suitable algorithms to each profile. In the literature there are several algorithms to extract the skeleton of the light line with sub-pixel accuracy.

Naidu and Fisher [58] reported a comparison of five algorithms, which are Gaussian approximation, center of mass, linear interpolation, parabolic estimator and Blais, and Rioux detectors. These algorithms can obtain the skeleton of the light line; however, the accuracy decreases if the light line does not have a uniform intensity distribution [18, 64]. This distribution can lose uniformity due to the shape of the object or when the light line is not perpendicular to the projected plane [65]. The gray-gravity method is widely applied due to its simple operation and fast calculation speed, but it is particularly sensitive to noise, resulting in lower accuracy [66, 67]. In reference [14], the algorithms based on the Gaussian approximation method, the least-squares, and Bezier curves are compared. The authors conclude that the algorithm based on Bezier curves, in terms of accuracy and processing time, it was more efficient. It is important to highlight that the algorithms mentioned above are based on the Gaussian profile of the laser line.

We will now describe three algorithms to obtain the skeleton of a light line based on the projected profile. According to the optical system described in section 1.2 (see Fig. 1.5.(a)), this captures one light line that extends along the rows of an image. The origin of the coordinates of the image is located in the pixel that is in the upper left position of the image. The pixels in the x-direction correspond to the columns and the pixels in the y-direction correspond to the rows of the image. The algorithms for obtaining the position of the maximum intensity value are applied in each one of column of the image. These algorithms are described below.

2.1 THE BEZIER CURVES METHOD

When the projection of a light line with a Gaussian profile is captured, it is convenient to adjust the intensity distribution of the pixels to a Bezier polynomial function [14].

The Bezier curves method allows to generate a continuous polynomial function that fits a set of pixels distributed transversely over the light line of the image captured, and the bisection method allows to find iteratively the position of the maximum intensity value of the function with sub-pixel accuracy. In our case, the skeleton of the light line is obtained by calculating the positions of maximum intensity along each column of the image. The Bezier polynomial function is mathematically represented by two parametric equations which relate the position and intensity of a set of pixels (x_0, z_0), (x_1, z_1), … (x_n, z_n). The two Bezier polynomial functions of n-degree are given by the following parametric equations:

$$x(u) = \sum_{i=0}^{n} \binom{n}{i} (1-u)^{n-i} u^i x_i, \qquad 0 \leq u \leq 1 \qquad (2.1)$$

$$z(u) = \sum_{i=0}^{n} \binom{n}{i} (1-u)^{n-i} u^i z_i, \qquad 0 \leq u \leq 1 \qquad (2.2)$$

Eqs. (2.1) and (2.2) allow to obtain a continuous function for sets of $(n+1)$ pixels; however, due to trial and error tests, and based on references [14, 16], choosing a set of 12 pixels is adequate to get the skeleton of each of the light line. Therefore, for a set of 12 pixels, the explicit equation of (2.1) and (2.2) is given by:

$$\begin{aligned} x(u) = {} & (1-u)^{11}x_0 + 11(1-u)^{10}ux_1 + \ 11(1-u)^{10}ux_1 + \\ & 55(1-u)^9u^2x_2 + 165(1-u)^8u^3x_3 + 330(1-u)^7u^4x_4 + \\ & 462(1-u)^6u^5x_5 + 462(1-u)^5u^6x_6 + 330(1-u)^4u^7x_7 + \\ & 165(1-u)^3u^8x_8 + 55(1-u)^2u^9x_9 + 11(1-u)u^{10}x_{10} + \\ & u^{11}x_{11}, \qquad 0 \leq u \leq 1 \end{aligned} \qquad (2.3)$$

$$\begin{aligned} z(u) = {} & (1-u)^{11}z_0 + 11(1-u)^{10}uz_1 + \ 11(1-u)^{10}uz_1 + \\ & 55(1-u)^9u^2z_2 + 165(1-u)^8u^3z_3 + 330(1-u)^7u^4z_4 + \\ & 462(1-u)^6u^5z_5 + 462(1-u)^5u^6z_6 + 330(1-u)^4u^7z_7 + \\ & 165(1-u)^3u^8z_8 + 55(1-u)^2u^9z_9 + 11(1-u)u^{10}z_{10} + \\ & u^{11}z_{11}, \qquad 0 \leq u \leq 1 \end{aligned} \qquad (2.4)$$

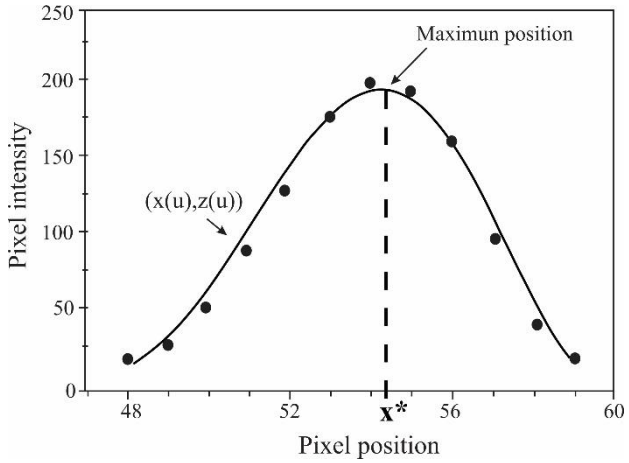

Figure 2.1. Position of maximum intensity of a set of pixels fitted to a Bezier function.

Fig. 2.1 shows a set of pixels fitted to a Bezier function. Due to the way in which the intensity of the pixels is distributed in each column of the image, to extract the position of maximum intensity (x^*) it is only necessary to calculate the value of u when $z'(u) = 0$. The mathematical expression of $z'(u)$ for a set of n pixels is given by:

$$z'(u) = \sum_{i=0}^{n} \binom{n}{i} (1-u)^{n-i-1} u^{i-1} (i - nu) z, \qquad 0 \le u \le 1 \quad (2.5)$$

For a set of 12 pixels, the explicit equation of (2.5) is given by:

$$\begin{aligned} z'(u) = {} & [-11(1-u)^{10}]z_0 + 11[(1-u)^9(1-11u)]z_1 + \\ & 55[(1-u)^8 u(2-11u)]z_2 + 165[(1-u)^7 u^2(3-11u)]z_3 + \\ & 330[(1-u)^6 u^3(4-11u)]z_4 + 462[(1-u)^5 u^4(5-11u)]z_5 + \\ & 462[(1-u)^4 u^5(6-11u)]z_6 + 330[(1-u)^3 u^6(7-11u)]z_7 + \\ & 165[(1-u)^2 u^7(8-11u)]z_8 + 55[(1-u)u^8(9-11u)]z_9 + \\ & 11[u^9(10-11u)]z_{10} + 11u^{10} z_{11}\,, \qquad 0 \le u \le 1 \end{aligned} \quad (2.6)$$

To extract x^* of a light line along columns, the bisection method proposed in references [14, 68] is implemented. For this algorithm, a pair of initial values are assigned. Since the function $z(u)$ is defined in the intervals $0 \le u \le 1$, then the assigned values are $u_i = 0$ and $u_s = 1$. The value u^* is half-way between u_i and u_s, i.e., $u^* = (u_i +$

$u_s)/2$. Using the general Eq. (2.5) (or Eq (2.6), for the case of 12 pairs of points), if $z'(u)$ evaluated in $u = u^*$ is positive, then $u_i = u^*$, else $u_s = u^*$. This calculation will be repeated until $(u_i - u_s) \approx 0$. Finally, the value of u^* is substituted in the general Eq. (2.1) (or Eq (2.3), for the case of 12 pairs of points) to find the position x^* of the function $x(u)$.

2.2 LINEAR REGRESSION METHOD

When the projection of a triangular profile light line is captured, it is possible to calculate the position of the maximum intensity value with sub-pixel accuracy by the linear regression method. Suppose that a set of *n* known data (x_i, y_i) can be adjusted to a simple straight-line model [69] given by:

$$z(x) = a + mx \tag{2.7}$$

where m is the slope of the $z(x)$ function, and a is the intercept with the z axis. The values of m and a are obtained by the following Eqs., respectively:

$$m = \frac{n\sum_{i=1}^{n} x_i z_i - \sum_{i=1}^{n} x_i \sum_{i=1}^{n} z_i}{n\sum_{i=1}^{n} x_i^2 - (\sum_{i=1}^{n} x_i)^2} \tag{2.8}$$

$$a = \frac{n\sum_{i=1}^{n} z_i - m\sum_{i=1}^{n} x_i}{n} \tag{2.9}$$

In this case, to extract x^*, the intensity distribution is fitted to two functions lines $z_1(x)$ and $z_2(x)$, as shown in Fig. (2.2). This procedure is simple, $z_1(x)$ and $z_2(x)$ are define as:

$$z_1(x) = a_1 + m_1 x \tag{2.10}$$

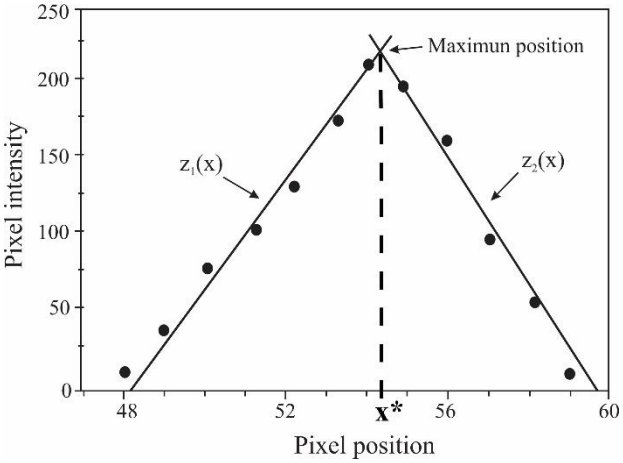

Figure 2.2. Position of maximum intensity of a set of pixels fitted to two linear functions.

$$z_2(x) = a_2 - m_2 x \tag{2.11}$$

where the values of m_1 and m_2 are obtained from Eq. (2.8), and the values of a_1 and a_2 from Eq. (2.9). Hence, the values x^* are determined by the point of intersection of the functions, i.e., when $z_1(x) = z_2(x)$ evaluated in $x = x^*$.

$$x^* = \frac{a_2 - a_1}{m_2 + m_1} \tag{2.12}$$

It is important to highlight that the values of x^* are obtained directly by the linear regression method (Eq. (2.12)), and not by iterative methods, which allows to considerably reduce the computational load.

2.3 NONLINEAR REGRESSION METHOD

When the projection of a sinusoidal profile light line is captured, it is possible to calculate the position of the maximum intensity value with sub-pixel accuracy by the nonlinear regression method.

A detailed description for fitting a distribution of n data pairs (x_i, y_i) to a sinusoidal function, as shown in Fig. 2.3, is found in reference [70]. A sinusoidal function is expressed mathematically as:

$$z(x) = asin(bx + c) + d \qquad (2.13)$$

where a, b, c and d are real constants. Fitting the values to a sine function brings the disadvantage that a nonlinear system of equations has to be solved to find the real constants, which increases the computational load critically. Using Newton's method, it is possible to find these constants iteratively. If it is defined that the real constants belong to a vector given by $\varepsilon = [a \quad b \quad c \quad d]^T$ (where $[\,.\,]^T$ denotes the transpose), then approximate values to ε are calculated by the following equation:

$$\varepsilon_{k+1} = \varepsilon_k + \frac{F(\varepsilon_k)}{J(\varepsilon_k)}; \quad k = 0, 1, 2, \ldots \qquad (2.14)$$

where $F(F \in M_n)$ is the vector field; $J(J \in M_n)$ is the Jacobian; $\varepsilon_k(\varepsilon_k \in M_{nx1})$ are values close to the neighborhood of a, b, c and d; and $\varepsilon_{k+1}(\varepsilon_{k+1} \in M_{nx1})$ are the new values of ε_k. Each term of Eq. (2.14) is expressed as:

$$\varepsilon_{k+1} = \begin{bmatrix} a_{k+1} \\ b_{k+1} \\ c_{k+1} \\ d_{k+1} \end{bmatrix}, \quad \varepsilon_k = \begin{bmatrix} a_k \\ b_k \\ c_k \\ d_k \end{bmatrix},$$

$$F = \begin{bmatrix} F_{11} & F_{12} & F_{13} & F_{14} \\ F_{21} & F_{22} & F_{23} & F_{24} \\ F_{31} & F_{32} & F_{33} & F_{34} \\ F_{41} & F_{42} & F_{43} & F_{44} \end{bmatrix}, \qquad (2.15)$$

$$J = \begin{bmatrix} J_{11} & J_{12} & J_{13} & J_{14} \\ J_{21} & J_{22} & J_{23} & J_{24} \\ J_{31} & J_{32} & J_{33} & J_{34} \\ J_{41} & J_{42} & J_{43} & J_{44} \end{bmatrix}$$

The details of the calculation of each element of the matrices F and J of the Eq. (2.15) is found in reference [70].

Newton's method initializes with the initial conditions, for $k = 0$, then $\varepsilon = [a_0 \quad b_0 \quad c_0 \quad d_0]^T$, and the iterations ends when the condition $\varepsilon_{k+1} - \varepsilon_k \approx 0$ is fulfilled, i.e., when the values of a_{k+1}, b_{k+1}, c_{k+1} and d_{k+1} are approximate to a, b, c and d, respectively.

Fig. 2.3 shows a set of pixels fitted to a sinusoidal function. Due to the way in which the intensity of the pixels is distributed in each column of the image, to extract x^*, it is only necessary to calculate the value of x when the first derivative is zero, i.e., when $z'(x) = 0$, where:

$$z'(x) = abcos(bx + c) \qquad (2.16)$$

In this case, is also proposed the bisection method to find the value of x^* iteratively. Since the function $z(x)$ is defined in the intervals $x_0 \leq x \leq x_n$, then the assigned values are $x_i = x_0$ and $x_s = x_n$. The value x^* is half-way between x_i and x_s, i.e., $x^* = (x_i + x_s)/2$. Using the Eq. (2.16), if $z'(x)$ evaluated in $x = x^*$ is positive, then $x_i = x^*$, else $x_s = x^*$. This calculation will be repeated until $(x_i - x_s) \approx 0$.

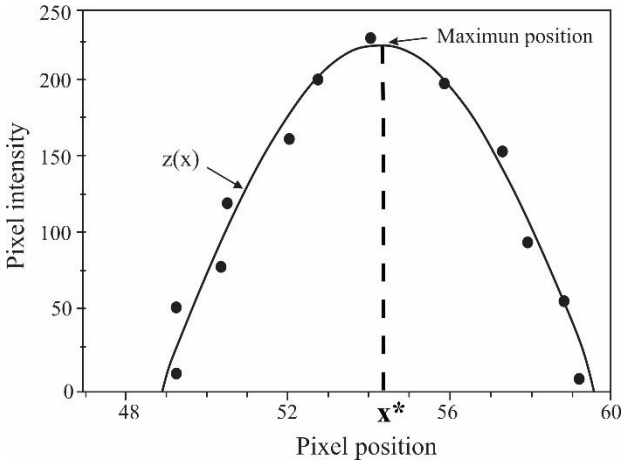

Figure 2.3. Position of maximum intensity of a set of pixels fitted to a sinusoidal function.

CHAPTER 3: 3D OBJECT SCANNING BY PROJECTION OF WHITE LIGHT PROFILES

In this chapter, we propose the 3D scanning of objects using the projection technique of a structured light line with different profiles. The profiles used were Gaussian, triangular and sinusoidal. Depending on the light profile used, the algorithms proposed in chapter 2 were implemented which are based on the Bezier curves, linear regression, and nonlinear regression methods. These algorithms allowed to obtain the skeleton of each line of light captured with sub-pixel accuracy. The use of a multimedia projector as a light source, instead of the traditional use of laser, has the advantage that the projected light line is free of the speckle pattern noise, which is one of the most important factors that deteriorate the images of the light line and consequently it has a negative impact on the measurements of the object dimensions [18, 21-24]. Other advantages are that the light profiles are easily generated and the optical arrangement for scanning objects easy to set up.

Three experiments were carried out for each projected light profile. The measurements of a test object were obtained using the proposed approach and the results were compared with the measurements obtained by a coordinate measuring machine (CMM).

Finally, the efficiency of each projected light profile used for scanning was determined in terms of accuracy and processing time.

3.1 EXPERIMENTAL SETUP

The experimental configuration of our scanning system by projection of one structured light line is shown in Fig. 3.1.(a). The system comprises a multimedia projector (resolution of 1280x800 pixels), a CCD camera (resolution of 640x480 pixels), and a computer. One light line with a certain profile (Gaussian, triangular or sinusoidal) is projected horizontally (y-direction) at an oblique angle to a reference plane. The light line moves vertically (x-direction) over the object surface which is placed on the reference plane. A camera placed perpendicular to the reference plane captures the light line when it moves in steps of one pixel through of the object surface. The computer (processor i7 3630QM of 2.40GHz, 64-bit operating system and a RAM memory of 8.0 GB) synchronizes the projection and capture of the light line, and it also allows to carry out

the processing of the images. The projector and the camera are separated from each other a distance d, and are placed regarding the reference plane at a distance D.

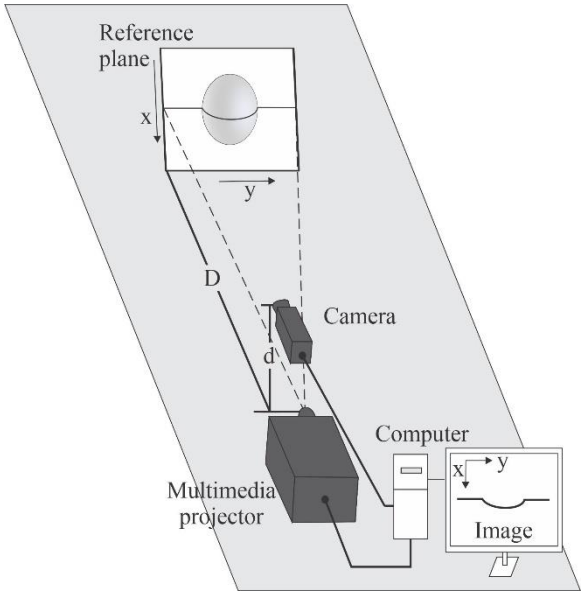

(a)

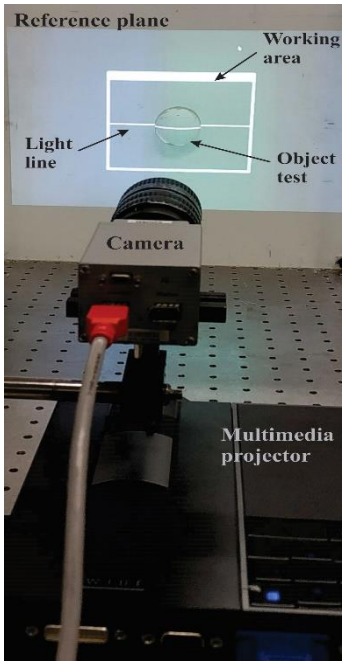

(b)

Figure 3.1. (a) Experimental setup scheme. **(b)** Photograph of the scanning system by projection of one light line.

The scanning system captures the images of the light line at a frequency of 30 fps, avoiding the use of mechanical systems compared to the LLP technique. The captured images were resized to 421x391 pixels to occupy only the surface of the object (Region of interest, see Fig. 3.1.(b)). A total of 200 images were captured for each experiment. The set of resized images was computationally processed using the algorithms proposed in chapter 2 for each one of the light profiles. Fig. 3.1.(b) shows the photograph of the scanning system by projection of one light line established.

The resolution along the light line (y-direction) is determined by the resolution of the camera, while the resolution in the other direction is determined by the number of light lines projected (which is related to the resolution of the projector). To obtain the resolution in the x and y direction in units of millimeters, it is necessary to calculate the pixels size of the captured images, for this, the width of these were measured, as shown in Fig. 3.2. The width in the horizontal direction was determined to be 57 mm for 391 pixels; therefore, the pixel size is equal to 0.145 mm. The value of 0.145 mm is the resolution in the y-direction. However, to obtain the resolution in the x-direction it is necessary to measure the number of pixels of the light line when it is moved from one position to another on the reference plane. Fig. 3.3.(a) shows the result of the superposition of two images of the light line on the reference plane. The upper line corresponds to the initial scan position of the light line (first image captured), and the lower line corresponds to the final scan position (last image captured). Fig. 3.3.(b) shows the positions in pixels of the maximum light line intensity in the first image and the last image captured (image captures two hundred). Therefore, the light line has been moved 404 pixels in 199 steps. With these known values, the resolution in the x-direction is obtained by the following relationship:

$$R = \frac{(Movement\ of\ the\ light\ line\ in\ pixels)}{(number\ of\ steps)}\ (pixel\ size\ in\ mm) \qquad (3.1)$$

According to Eq. (3.1), the resolution in the x-direction is 0.29 mm.

Finally, the time it took for our system to capture the 200 images was 6.67 s. The values of D and d were obtained with a measuring tape and whose values are 634.0 mm and 157.0 mm, respectively.

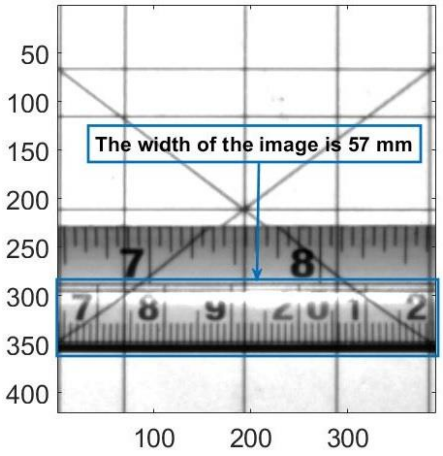

Figure 3.2. Measurement in mm in the y-direction of the region of interest to calculate the pixel size.

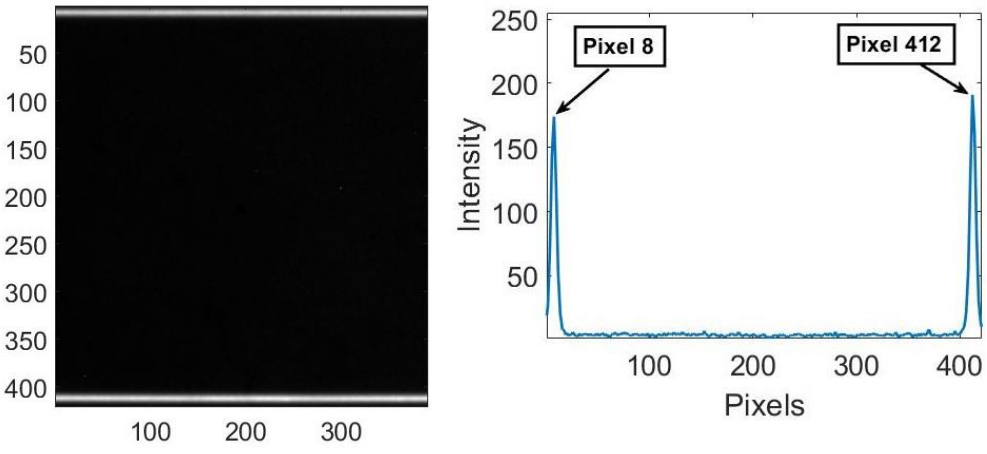

(a) (b)

Figure 3.3. (a) Result of the superposition of the light line of the first image captured (upper line), and the image 200 captured (lower line). **(b)** Positions in pixels of the maximum light line intensity in the first image and in image 200.

The test object used in our experiment is shown in Fig. 3.4. Measurements of the height differences on the test object of eight lateral points (indicated by the circles) with respect to a central point (indicated by the rectangle) were measured in three experiments with scanning system by projection of one light line. In each experiment, one light line with Gaussian, triangular and sinusoidal profile was projected, respectively. The results obtained by our scanning system were compared with those obtained by a coordinate measuring machine (CMM). The experimental results are shown below.

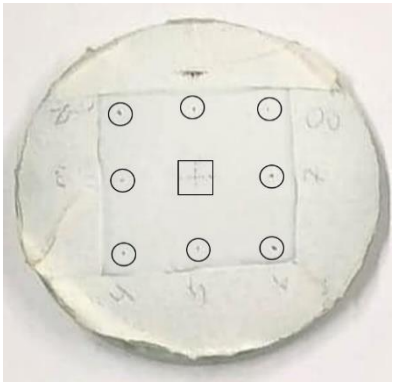

Figure 3.4. Test object for reconstruction. The heights of the points indicated by the circles were measured with respect to the point indicated by the rectangle.

3.2 EXPERIMENTAL RESULTS

Firstly, it is important to highlight that in the three experiments carried out, the images captured from the light line were free of speckle noise, so it was not necessary to implement digital filters in the image processing. Therefore, compared to the LLP technique, our proposal avoids the speckle noise which is one of the main factors that reduce the accuracy of measurements and increases the processing time[21, 23, 24]. Some of the captured images for each captured light profile are shown in Figs. 3.5.(a), 3.6.(a) and 3.7.(a).

3.2.1 Results of the projection of light with a Gaussian profile

In this case, to obtain the skeleton of the captured images of the light lines, the Bezier curves method described in section 2.1 was implemented.

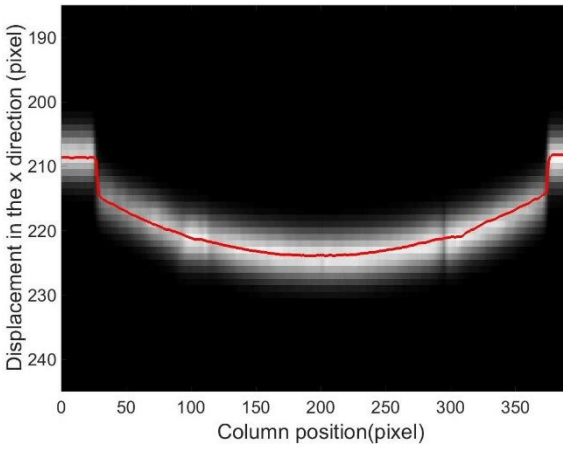

(a)

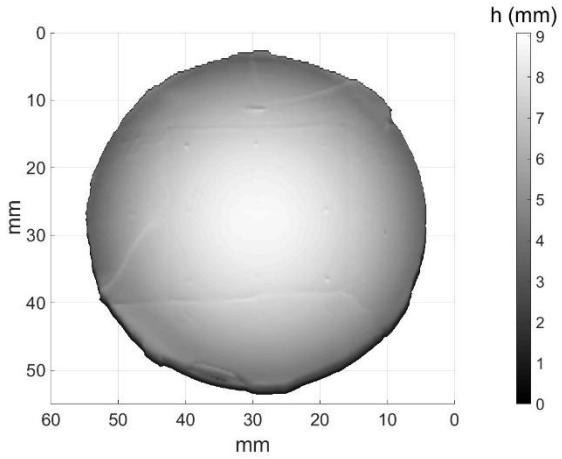

(b)

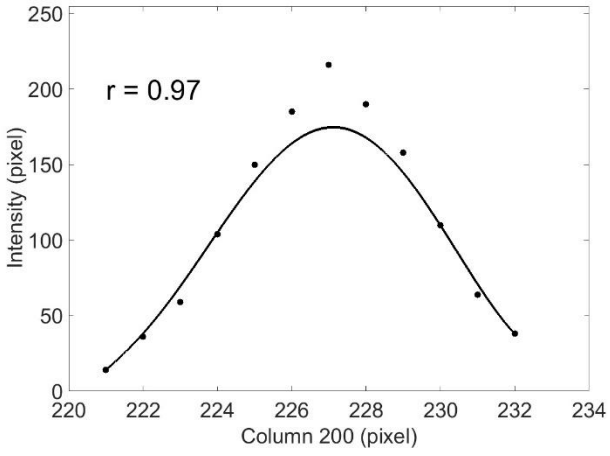

(c)

Figure 3.5. (a) Capture of the projected light line with Gaussian profile and its skeleton (red line). **(b)** Intensity distribution of the light line profile along column 200 (black spots) fitted to a continuous Bezier function (continuous black line). **(c)** 3D reconstruction of a test object.

Fig. 3.5.(a) shows one of the captured images of the light line with Gaussian profile. The intensity distribution of the light line (black spots) is shown in Fig. 3.5.(b), which was obtained along column 200 of the image of the Fig. 3.5.(a). This distribution is fitted to a Bezier polynomial function (continuous black line) and whose correlation coefficient is $r = 0.97$, which demonstrates high confidence in the fit. The positions of maximum intensity of the light lines in the captured images were calculated by the bisection method. The skeleton of the light line of the image in question is shown in Fig. 3.5.(a) (red line); took an average processing time of 0.1498 s. Afterward, the skeleton calculation of the light lines for all the images captured was carried out, which allowed obtaining the displacements $s(x, y)$ with respect to the projections made on the reference plane and the heights $h(x, y)$ of the test object by Eq. (1.5); this took a processing time of 7.1773 s. The 3D shape of the test object is shown in Fig. 3.5.(c). Table 3.1 summarizes the absolute error of each measurement made on the test object, and the average absolute error for the projected Gaussian light profile whose value is 0.0534 mm.

Table 3.1. Heights difference of eight lateral points considered in the measurements of the test object with respect to a central point (see Fig. 3.4) measured with scanning system by projection of one light line with Gaussian profile and by the CMM.

Measurements	Scanning system (mm)	CMM (mm)	Absolute error (mm)
1	1.0240	1.0137	0.0103
2	1.9070	1.9693	0.0623
3	1.0060	0.9418	0.0642
4	1.7240	1.7811	0.0571
5	0.8980	0.8276	0.0704
6	1.7880	1.7418	0.0462
7	0.8980	0.9445	0.0465
8	1.7240	1.7938	0.0698

Average absolute error: 0.0534 mm.

3.2.2 Results of the projection of light with a triangular profile

In this case, to obtain the skeleton of the captured images of the light lines, the linear regression method described in section 2.2 was implemented.

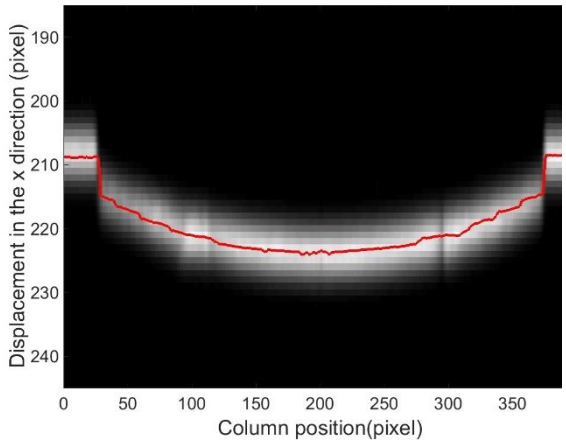

(a)

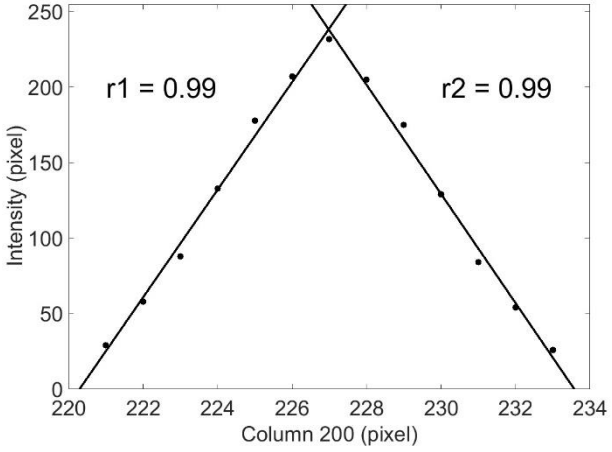

(b)

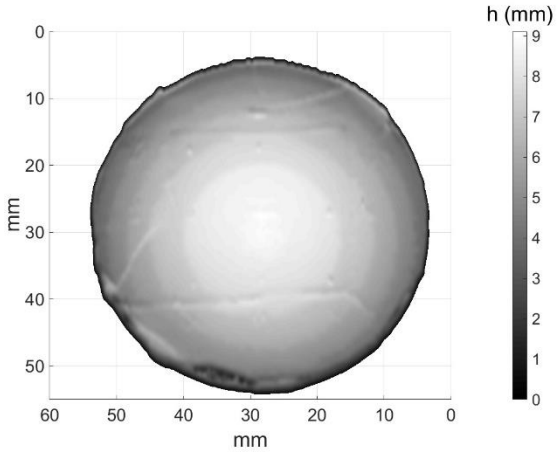

(c)

Figure 3.6. (a) Capture of the projected light line with triangular profile and its skeleton (red line). **(b)** Intensity distribution of the light line profile along column 200 (black spots) fitted to two triangular functions (continuous black line). **(c)** 3D reconstruction of a test object.

Fig. 3.6.(a) shows one of the captured images of the light line with triangular profile. The intensity distribution of the light line is shown in Fig. 3.6.(b), which was obtained along column 200 (black spots). This distribution is fitted to two linear functions (continuous black line) and whose correlation coefficients are $r_1 = 0.99$ and $r_2 = 0.99$ for the function with slope m_1 and m_2, respectively. The correlation coefficients demonstrate high confidence in the fit. Through the direct use of Eq. (2.12), the positions of maximum intensity of the light line were calculated. The skeleton of the light line of the image in question is shown in Fig. 3.6.(a) (red line); took an average processing time of 0.0752 s. Later, the displacements $S(x, y)$ of the light lines for all the images captured with respect to the projections made on the reference plane, and the heights $h(x, y)$ of the test object were calculated, this took an average processing time of 2.5946 s. The 3D shape of the test object is shown in Fig. 3.6.(c). Table 3.2 summarizes the absolute error of each measurement made on the test object, and the average absolute error for the projected triangular light profile whose value is 0.1616 mm.

Table 3.2. Heights difference of eight lateral points considered in the measurements of the test object with respect to a central point (see Fig. 3.4) measured with scanning system by projection of one light line with triangular profile and by the CMM.

Measurements	Scanning system (mm)	CMM (mm)	Absolute error (mm)
1	0.8020	1.0137	0.2117
2	1.8400	1.9693	0.1293
3	0.9418	0.9418	0.0498
4	1.6860	1.7811	0.0951
5	0.6170	0.8276	0.2106
6	1.7570	1.7418	0.0152
7	0.5670	0.9445	0.3775
8	1.9970	1.7938	0.2032

Average absolute error: 0.1616 mm.

3.2.3 Results of the projection of light with a sinusoidal profile

In this case, to obtain the skeleton of the captured images of the light lines, the nonlinear regression method described in section 2.3 was implemented.

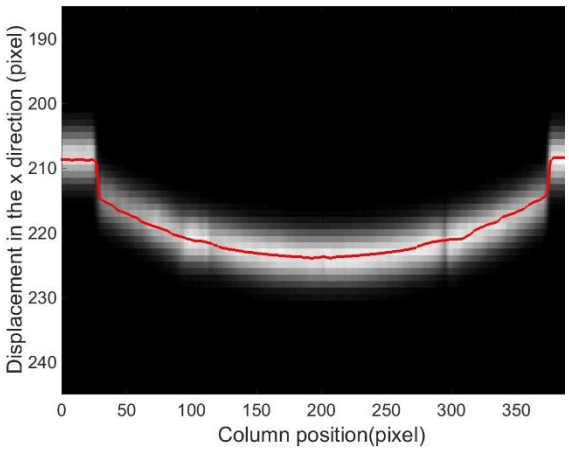

(a)

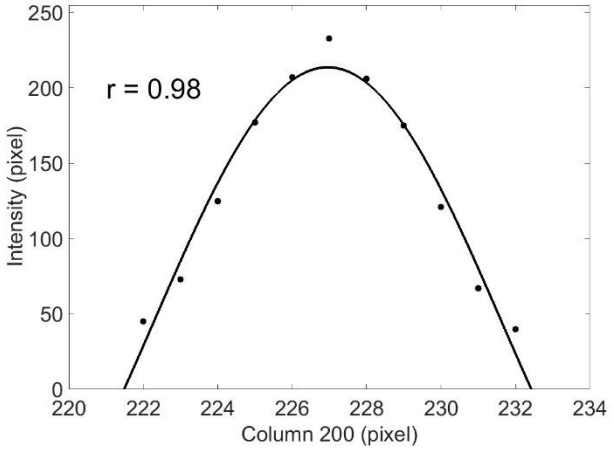

(b)

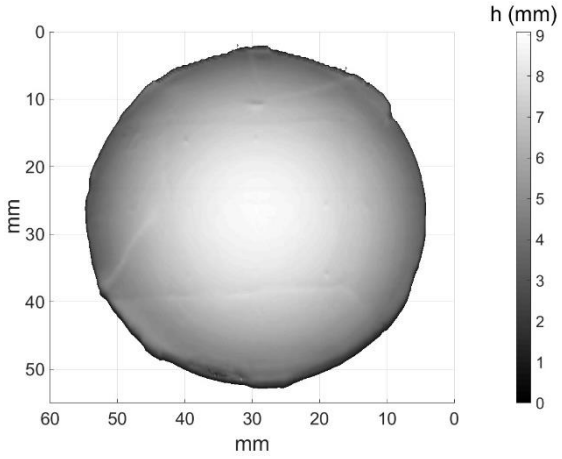

(c)

Figure 3.7. (a) Capture of the projected light line with sinusoidal profile and its skeleton (red line). **(b)** Intensity distribution of the light line profile along column 200 (black spots) fitted to a sinusoidal function (continuous black line). **(c)** 3D reconstruction of a test object.

Fig. 3.7.(a) shows one of the captured images of the light line with sinusoidal profile. The intensity distribution of the light line is shown in Fig. 3.7.(b), which was obtained along column 200 (black spots). This distribution is fitted to sinusoidal functions (continuous black line) whose correlation coefficient is $r_1 = 0.98$, which demonstrates high confidence in the fit. The positions of maximum intensity of the light line were calculated by the bisection method. The skeleton of the light line in question is shown in Fig. 3.7.(a) (red line); took an average processing time of 0.2707 s. Analogously to previous experiments, the displacements $S(x, y)$ and heights $h(x, y)$ of the test object were calculated, which took an average processing time of 2.5946 s. The 3D shape of the test object is shown in Fig. 3.7.(c). Table 3.3 summarizes the absolute error of each measurement made on the test object, and the average absolute error for the projected sinusoidal light profile whose value is 0.0559 mm.

Table 3.3. Heights difference of eight lateral points considered in the measurements of the test object with respect to a central point (see Fig. 3.4) measured with scanning system by projection of one light line with sinusoidal profile and by the CMM.

Measurements	Scanning system (mm)	CMM (mm)	Absolute error (mm)
1	0.9660	1.0137	0.0477
2	1.9220	1.9693	0.0473
3	0.9760	0.9418	0.0342
4	1.7020	1.7811	0.0791
5	0.7810	0.8276	0.0466
6	1.8280	1.7418	0.0862
7	0.9930	0.9445	0.0485
8	1.7360	1.7938	0.0578

Average absolute error: 0.0559 mm.

3.3 DISCUSSION OF THE RESULTS

Table 3.4 summarizes the correlation coefficients, the processing time to skeletonize one light line, and the processing time it took for each algorithm to get the 3D shape of the test object for each projected light profile.

Table 3.4. Summary values of correlation coefficient, processing time for skeletonize one light line and processing time to obtain the 3D shape of the object for each projected light line profile and its respective reconstruction algorithms.

Projected light profile	Algorithms	Correlation coefficient	Process time for one line (s)	Time to obtain the 3D shape of the object (s)
Gaussian	Bezier curves method	0.97	0.1498±0.0012	7.1773±0.0404
Triangular	Linear regression method	0.99	0.0752±0.0013	2.5946±0.0283
Sinusoidal	Nonlinear regression method	0.98	0.2707±0.0097	41.2671±0.2016

Using the Bezier curves method, a slightly lower correlation coefficient was obtained regarding the other two methods. However, this method is more robust in calculating the maximum intensity positions when the intensity distribution of the light line is not uniform, therefore, it presents greater robustness when the light line is projected on abrupt variations in the object's surface. Through this method, the average absolute error obtained was smaller than the other two methods and whose value was 0.0534 mm, while the processing time to get the 3D shape of the object was 7.1773 s.

Using the linear regression method, a correlation coefficient of 0.99 was obtained, whose value is slightly higher regarding the other two methods. However, the values of the positions of maximum intensity are very sensitive to the values of the slopes m_1 and m_2. For example, these positions have a variation of two pixels if the values of the slopes m_1 or m_2 are modified in one unit, which has a negative impact that directly influences the accuracy of the measurements. This problem becomes more serious when the intensity distribution of the light line is not uniform in the captured image. Consequently, this method has an average absolute error value equal to 0.1616 mm, which is higher than the other methods. The main advantage of the method is the processing time whose value, shown in table 3.4, is much smaller than the other two methods, which allows its

application in situations where high speed is required to obtain the 3D shape of objects in case high accuracy in measurements is not a critical requirement.

Using the nonlinear regression method was obtained an average absolute error equal to 0.0559 mm. Although this result is approximate compared to the Bezier curve method; however, when obtaining the 3D shape of the object, the processing time was much longer (41.2671 s). An example of application is that this method can be complemented to the proposal carried out in reference [26], where the 3D shape of an object is reconstructed by the single-shot technique, obtaining the phase map of a sinusoidal fringes pattern. In [26], the phase map is obtained by skeletonizing the fringes through the application of morphological operations, instead of the traditional PSP technique. In this case, it would be convenient to apply the nonlinear regression method to get the skeleton of the fringe pattern with sub-pixel accuracy, instead of morphological operations whose resolution is one pixel. Processing time is expected to be more efficient due to a single image is processed.

Figs. 3.8.(b), 3.8.(c), and 3.8.(d) show the result of the 3D scanning of an a second object under test (Fig. 3.8.(a)) by light line projection with a Gaussian, triangular and sinusoidal profile, respectively. Clearly, the surface of this irregular object is more complex than the first test object; however, the proposed methods work well with each reconstruction. Up to this point, it is important to mention that due to the smooth shape and dimensions of the object there was no need to deal with the problem of occluded lines. However, if in some reconstruction experiments of objects with complex geometry, occluded lines with small discontinuities were obtained, we recommend using interpolation methods to connect the broken lines of the object image as proposed in the references [61, 68]. In the case of long discontinuities, we recommend avoiding the reconstruction of the occluded zone, since the methods of interpolation will inevitably fail.

Finally, the 3D scanning technique by projection of one light line using a projector as a source of light, allows us to obtain the shape of objects with a very complex texture such as the third test object (pumice stone) shown in Fig. 3.9, where much of the surface detail is observed; or the fourth test object shown in Fig. 3.10, where it is observed fine details of the dental piece. These reconstructions were obtained by Gaussian light projection using the algorithms of section 2.1.

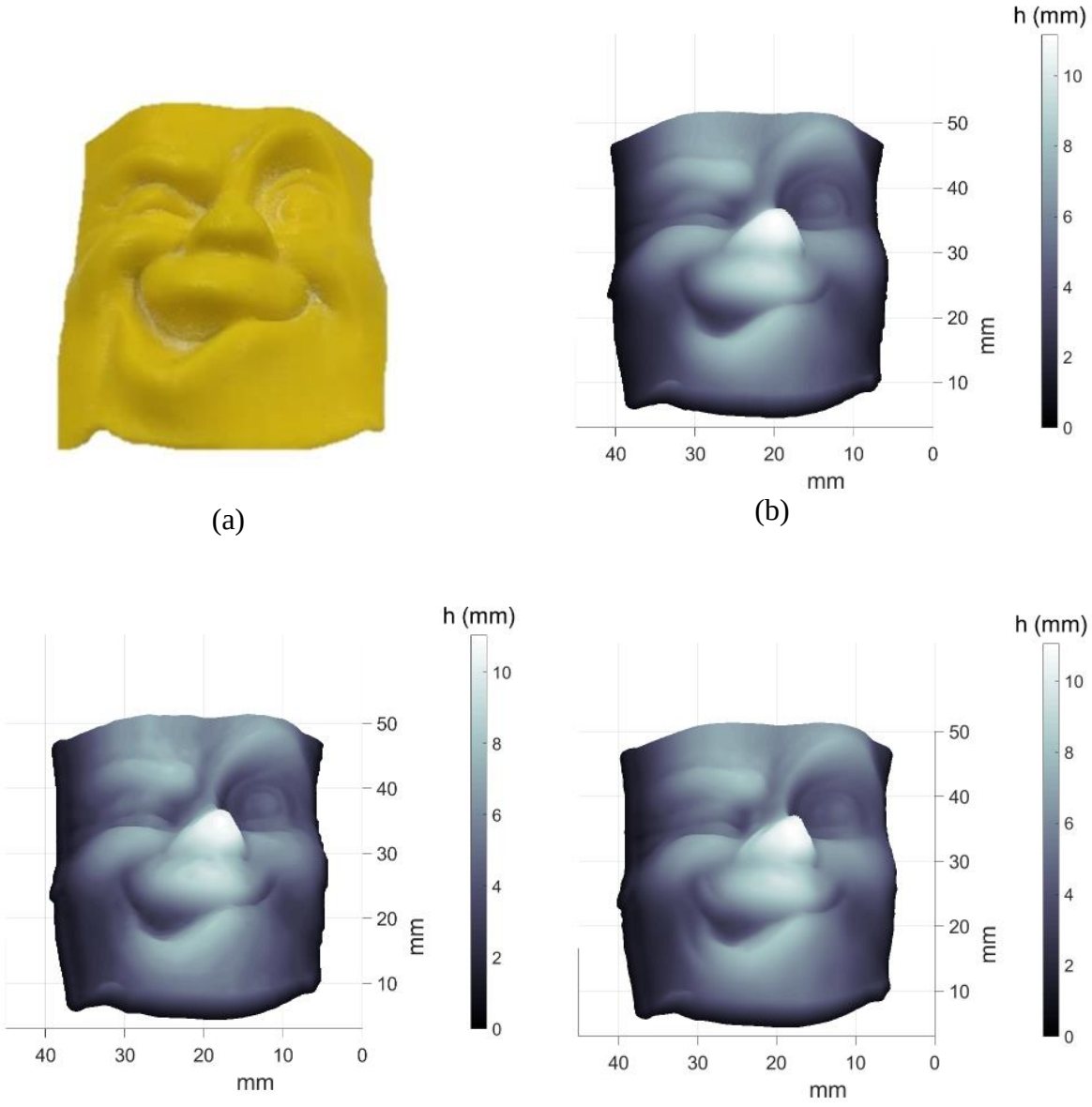

Figure 3.8. (a) 3D scanning of an irregular object by projection of one light line with **(b)** Gaussian profile, **(c)** triangular profile, and **(d)** sinusoidal profile.

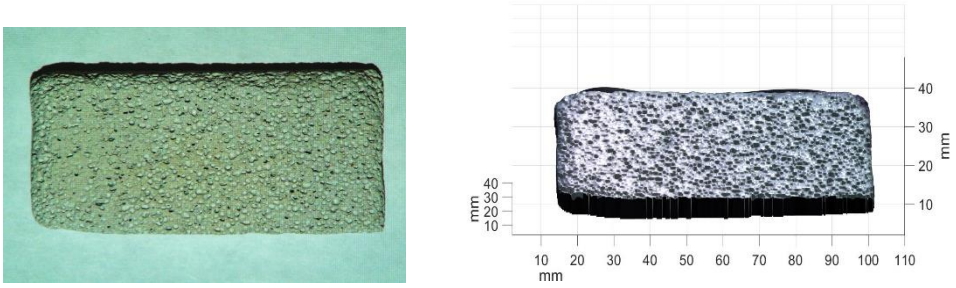

(a) (b)

Figure 3.9. (a) Sample of a pumice stone. **(b)** 3D scanning of the sample of a pumice stone.

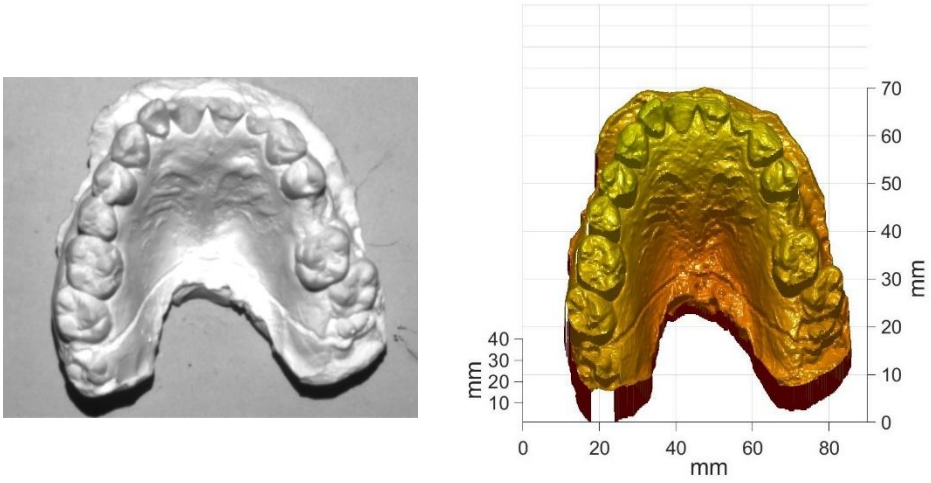

(a) (b)

Figure 3.10. (a) Sample of a dental piece. **(b)** 3D scanning of the sample of the dental piece.

The major contribution of this chapter includes:

1. The use of a multimedia projector to digitally generate different types of structured light profiles (Gaussian, triangular and sinusoidal), avoiding speckle noise, and making mechanical implementation simpler compared to laser line projection technique.
2. To implement different algorithms to obtain the skeleton of the light lines, such as linear regression method and nonlinear regression method and not be limited to algorithms based on the Gaussian profile when using the laser line projection technique.
3. Avoiding speckled noise made it possible to dispense with the implementation of complex digital filter algorithms.
4. As well as the laser line projection technique, our proposal allows obtain information of each pixel of the image and relate it to the object surface.

Finally, use a multimedia projector as a light source will allow leading to new research work where it is possible to control the light line intensity based on the local reflectivity of the object surface. This would greatly reduce discontinuities caused by low illumination, and improve the contrast of the light lines. This proposed work will make more efficient the three-dimensional measurement of an object.

3.4 CONCLUSIONS

In this chapter, the projection of different types of structured light profiles was proposed to obtain the 3D shape of objects, such as Gaussian, triangular and sinusoidal profiles. To obtain the light line skeleton, an appropriate algorithm for each type of projected profile was implemented. According to the results, the method based on the Bezier curves combined with the bisection method applied to light projection with Gaussian profile, allows obtaining greater accuracy in the measurements of the test object regarding the other two methods studied. In terms of processing time, the use of the linear regression method applied to light projection with triangular profile gets faster results compared to the other two methods. Therefore, it could be conveniently applied in situations where high accuracy is not required, for example in the field of archeology. On the other hand, although the processing time is very long when the nonlinear regression method combined with the bisection method is used with projected sinusoidal profiles, it can be applied in single-shot structured light line pattern techniques as proposed in

reference [26]. In this reference, 3D shapes of objects could be obtained by skeletonizing the sinusoidal fringe pattern with sub-pixel accuracy using the nonlinear regression method, instead of the traditional phase shifting profilometry technique.

Therefore, the criteria for choosing the suitable projected light profile for obtaining 3D shapes of objects will depend on the requirements and need of the application, either speed of measurement or high accuracy of it.

CHAPTER 4: 3D SCANNING OF OBJECTS BY PROJECTION OF THREE COLOR LINES WITH GAUSSIAN PROFILE

In this chapter, we will extend the study of our previous work [16], described in the chapter 3. We propose the 3D scanning of objects using the simultaneous projection of three color lines (red, green, and blue) with Gaussian profile. These lines scan simultaneously different zones of the test object with the purpose of optimizing the capture time and the number of stored images, compared to projection one light line. To carry out our proposal, we will take advantage of the RGB color channels of the CCD camera and segment each color line into the corresponding color channel. In this way, each line will be able to independently scan, in each color channel, different zones of the object simultaneously, then these scanned zones will be assembled to obtain the complete 3D shape of the object. It is worth mentioning that we will use a color segmentation method, based on reference [71], that does not require establishing threshold values, which allows an unsupervised operation. Additionally, the projected color lines profile is of the Gaussian type with the purpose carry out the skeletonization process using the Bezier polynomial method combined with the bisection method, which allows obtaining better results of the 3D reconstruction in terms of accuracy and processing time [14, 16]. Finally, although our proposal is limited to the application of static objects, it allows scanning objects with great measurement depths since it lacks the problem of ambiguity of the projected lines, obtaining a high density of reconstructed pixels.

4.1 FRAMEWORK AND ARCHITECTURE

Our proposal for 3D scanning of objects by the projection of three color lines is shown in the scheme of Fig. 4.1. The three color lines projected (red, green, and blue) will independently scan, in steps of one pixel, different zones of a test object surface which is placed on a reference plane. The reference plane is divided into three zones of equal dimensions. Each zone of the reference plane belongs to a zone of the test object that is scanned by one color line, that is, (according to Fig. 4.1) the red line scans the zone of the object that belongs to the zone of the reference plane bounded by points 1 and 2. The same way, the green line scans the zone of the object that belongs to the zone of the reference plane bounded by points 2 and 3, and finally, the blue line scans the zone of the object that belongs to the zone of the reference plane bounded by points 3 and 4.

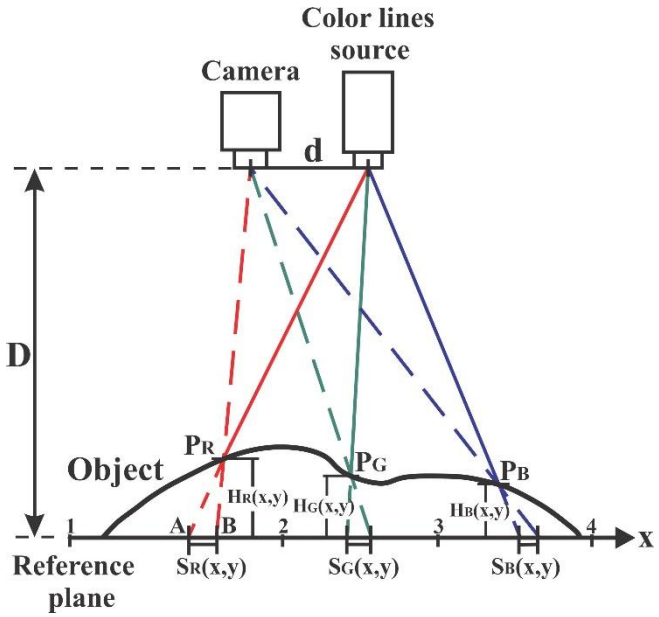

Figure 4.1. Geometric schema of the projection system of three color lines.

The optical geometry of the proposed scanning system is composed of a color CCD camera and a multimedia projector which are placed at a distance d from each other and located at a distance D from the reference plane. According to Fig. 4.1, when there is no object, the ray from the red light line impinges upon the point A from the reference plane. Once the test object is placed, the same ray impinges upon the point P_R. Hence, the ray from the red light line in the reference plane has been displaced from A to B. This displacement is captured in an image by the color CCD camera, and is represented by $S_R(x,y)$ in units of pixels. An analogous displacement is given for each light ray from the green and blue line, which impinge on the points P_G and P_B; in this case the displacements are represented by $S_G(x,y)$ and $S_B(x,y)$ in units of pixels, respectively. According to references [14, 16], the displacements $S_R(x,y)$, $S_G(x,y)$ and $S_B(x,y)$, after being converted to real units, are related to the height of the object by the following equation:

$$H_i(x,y) = \frac{DS_i(x,y)}{d + S_i(x,y)}, \qquad i = R, G \text{ and } B \quad (4.1)$$

Similar to the procedure developed in section 3.1, to order to get the measurements of the displacements for all the pixels of the color light lines projected, it is necessary to extract the skeleton of the captured images. However, now the scanning system captures RGB images that are previously processed in each color channel with the purpose of segmenting the color lines and subsequently carrying out skeletonization independently in grayscale (in each channel), as we will see in the next section.

Finally, according to the conclusions obtained in the chapter 3 and references [14, 16], it is convenient, in terms of accuracy and processing time, to get the skeleton through the Bezier curves method combined with the bisection method. The data obtained from the displacements of each skeleton is stored in a matrix memory to finally get the 3D shape of objects.

4.2 LINES SEGMENTATION BY COLOR

Segmentation of an image consists of grouping pixels based on specific features of the objects to be recognized. Some of the main factors that reduce the effectiveness of segmentation algorithms when using 3D reconstruction techniques by projection of color lines, are related to reflectance of the object (albedo), ambient light, the color of the object, projector illumination, cross-talk color, and so forth [72-74]. When these factors are combined, the projected color lines on the object modify its characteristics in such a way that it makes segmentation by color is difficult and the algorithms inevitably fail in many cases, so identifying the color lines is not a trivial task. In references [71, 75-77], original solutions are provided to get good results in the segmentation of color lines under the influence of ambient light and the color saturation of the object in question. In order to get robustness in the lines segmentation by color and can obtain the 3D shape of objects with slightly saturated colors, we are based on the proposal of reference [71], which suggests capturing an additional image to later carry out the segmentation process.

In our experiment, three color lines (red, green, and blue) are projected (see Fig. 4.1), which allow different zones of the object to be scanned simultaneously. The irradiance of the image generated by the multimedia projector in the CCD camera can be represented as:

$$I(\lambda) = g_{\theta} S(\lambda) E(\lambda) \qquad (4.2)$$

where λ is the wavelength, $S(\lambda)$ is the object reflectance, E(λ) is the illumination from the projector, and g_θ is the geometric shading factor determined by the surface orientation and illumination angle.

The captured image of the illuminated object with the color lines (I_1), and another captured image of the object illuminated displaced a certain number of pixel (I_2), can be represented as:

$$I_1(\lambda) = g_\theta S(\lambda)[E_1(\lambda) + A(\lambda)] \tag{4.3}$$

$$I_2(\lambda) = g_\theta S(\lambda)[E_2(\lambda) + A(\lambda)] \tag{4.4}$$

where the effect of ambient illumination $A(\lambda)$ is included in Eq. (4.3) and Eq. (4.4). Since g_θ depends on the geometry of the optical arrangement and $S(\lambda)$ depends on the properties of the object, then, g_θ and $S(\lambda)$ are assumed to be constant. Under these conditions, one way to remove the illumination of the background light of the projector is by differing the two previously captured images:

$$\begin{aligned} \Delta I(\lambda) &= I_1(\lambda) - I_2(\lambda) \\ &= g_\theta S(\lambda) \Delta E(\lambda) \end{aligned} \tag{4.5}$$

Similarly, the ambient illumination in each channel of an image can be removed by the following equations:

$$\Delta R = g_\theta S^R \Delta E^R \tag{4.6}$$

$$\Delta G = g_\theta S^G \Delta E^G \tag{4.7}$$

$$\Delta B = g_\theta S^B \Delta E^B \qquad (4.8)$$

where S^R, S^G y S^B are the reflectances of the object in the R, G y B channels, respectively. E^R, E^G y E^B are the illumination from the projector in the R, G y B channels, respectively. The application of Eqs. (4.6), (4.7), and (4.8) we will be able to segment the images of the color lines captured by the CCD camera. Although in most cases this simple segmentation procedure works well, it is possible that the image of the segmented light line includes small areas with illuminated pixels that do not belong to the light line. If this happens, this problem is easily solved by using the morphological operation of opening [78].

Finally, after segmenting the images in each color channel (R, G, and B), the next process is to skeletonize each color line by determining the positions of the pixels of maximum intensity. The skeletonization of the light lines is carried out by the bisection method described in section 2.1, which will allow us to obtain the positions of the pixels of maximum intensity with sub-pixel accuracy. The results are shown in section 4.5.

4.3 EXPERIMENTAL SETUP

A schematic of the experimental setup of our scanning system by the projection of three color lines with Gaussian profile is shown in Fig. 4.2.(a), which comprises a multimedia projector, a color CCD camera, and a computer.

The projector generates three color lines that are projected horizontally (y-direction, see Fig. 4.2.(a)) at an oblique angle to the reference plane. Scanning of an object placed in front of a reference plane is carried out by moving vertically (x-direction) each color line in steps of one pixel. In our experiments was used a multimedia projector DELL 1609WX which can project images with a resolution of 1280x800 pixels It should be mentioned that the color lines were projected onto a work area (see Fig. 4.2.(b)) which can vary in dimensions based on the size of the object to be reconstructed.

The camera is placed perpendicular to the reference plane and captures the images of the projected color lines while these scanning the object. In our experiments was used a color CCD camera that capture the images with a resolution of 1536x2048 pixels. For the

case of the test object shown in Fig. (4.3), the captured images were cropped to 1374x762 pixels to occupy only the region of interest (ROI) of the object to be reconstructed.

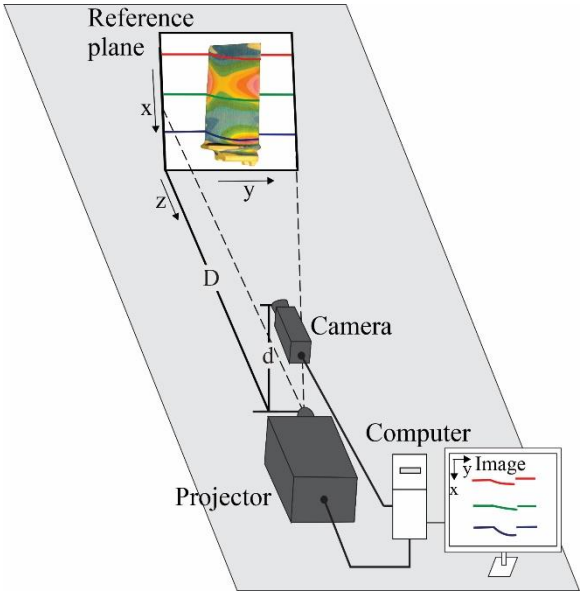

(a)

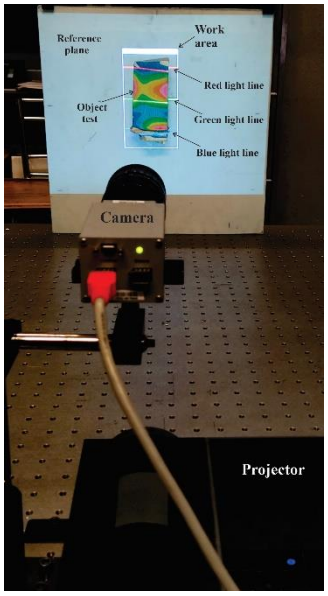

(b)

Figure 4.2. (a) Experimental setup scheme. **(b)** Photograph of the scanning system by projection of three color lines.

The computer allows the synchronization between the projection and the capture of the color lines. To obtain the 3D shape of the test object (Fig. 4.3), the scanning system captured a total of 180 images at a rate of 30 fps; the capture time of all images was 6 s.

Figure 4.3. Colored test object.

Similar to the experimental setup used in section 3.1, the resolution along the light line (y-direction) is determined by the pixel size in units of millimeters. According to Fig. 4.4, it was determined that the width of the image is 89 mm which is equivalent to 762 pixels; therefore, the lateral resolution in the y-direction is 0.1168 mm. To obtain the resolution in the x-direction, the number of pixels of the green light line was measured when it is moved from one position to another on the reference plane. Fig. 4.5.(a) shows the result of the superposition of two images of the green light line on the reference plane. The upper line corresponds to the initial scan position of the green light line (first image captured), and the lower line corresponds to the final scan position (last image captured). Fig. 4.5.(b) shows the positions in pixels of the maximum intensity of the green light line in the first image and the last image captured (image captured 180). Therefore, the light line has been moved 462 pixels in 179 steps. With these known values, the resolution in the x-direction is obtained by Eq. (3.1). The lateral resolution in the x-direction is 0.30 mm.

Finally, the values of D and d were obtained with a measuring tape and whose values are 828.0 mm and 210.0 mm, respectively.

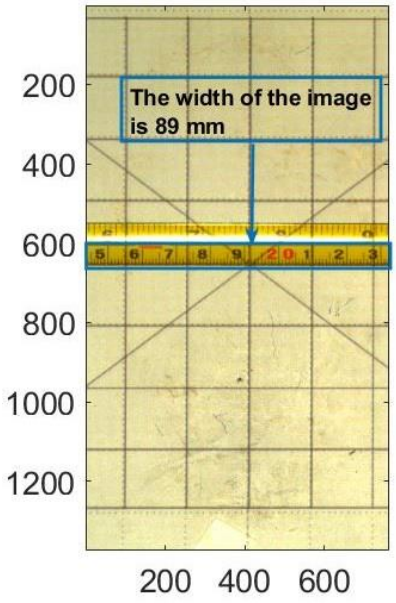

Figure 4.4. Measurement in mm in the y-direction of the region of interest to calculate the pixel size.

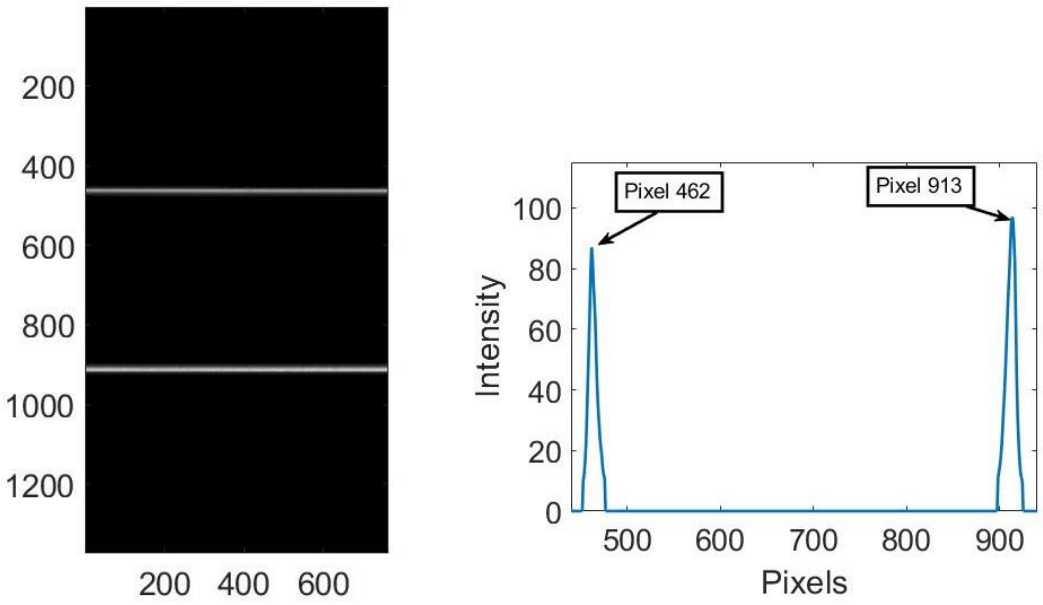

(a) (b)

Figure 4.5. (a) Result of the superposition of the green light line of the first image captured (upper line), and the image captured 180 (lower line). **(b)** Positions in pixels of the maximum intensity of the green light line of the first image and image captured 180.

4.4 RESULTS AND DISCUSSION

Firstly, it is important to highlight the capture time the number of images captured by our scanning system. If our scanning system had only projected one light line to obtain the 3D shape of the object in question, as carried out in reference [16], it would have registered a total of 540 images in a time of 18 s. For this reason, our scanning system allows us to optimize the time and the number of images captured; however, the price paid is the implementation of the segmentation algorithms by color. It is important to note that since in most cases the execution time of the segmentation algorithms are faster than the time to capture an image, the implementation of the segmentation algorithms does not provide a disadvantage in terms of processing time in the reconstruction of the object.

An important step for object scanning using the proposed approach is the process of color line segmentation of captured images. As mentioned above, some of the factors that decrease the effectiveness of segmentation methods are the color of the object's surface and ambient illumination. However, most applications are carried out in environments where usually illumination projected by the projector is much higher than the ambient illumination enters the CCD camera; hence, using a diaphragm is always possible to improve the contrast of the color lines by attenuating the light intensity. The use of the diaphragm in most cases is essential in the optical systems, because it prevents the CCD camera capture images with saturated zones due to the excessive light intensity that may come from the scene.

The test object is shown in Fig. 4.3, and whose surface has a color distribution that allows testing the efficiency of lines segmentation by color. Fig. 4.6.(a) shows a typical captured image by the color CCD camera; the test object is observed with the color lines projected on its surface. Figs. 4.6.(b), 4.6. (c), and 4.6. (d) show the results of the lines segmentation by color of the R, G, and B color channels in grayscale, respectively. It is noted the optimal results of the color segmentation algorithm implemented for our experiments, which are based on reference [71]. It is important to highlight the advantage of the procedure of lines segmentation by color, due to that it is not necessary to establish any type of threshold, allowing at this stage an unsupervised operation of the proposed scanning system.

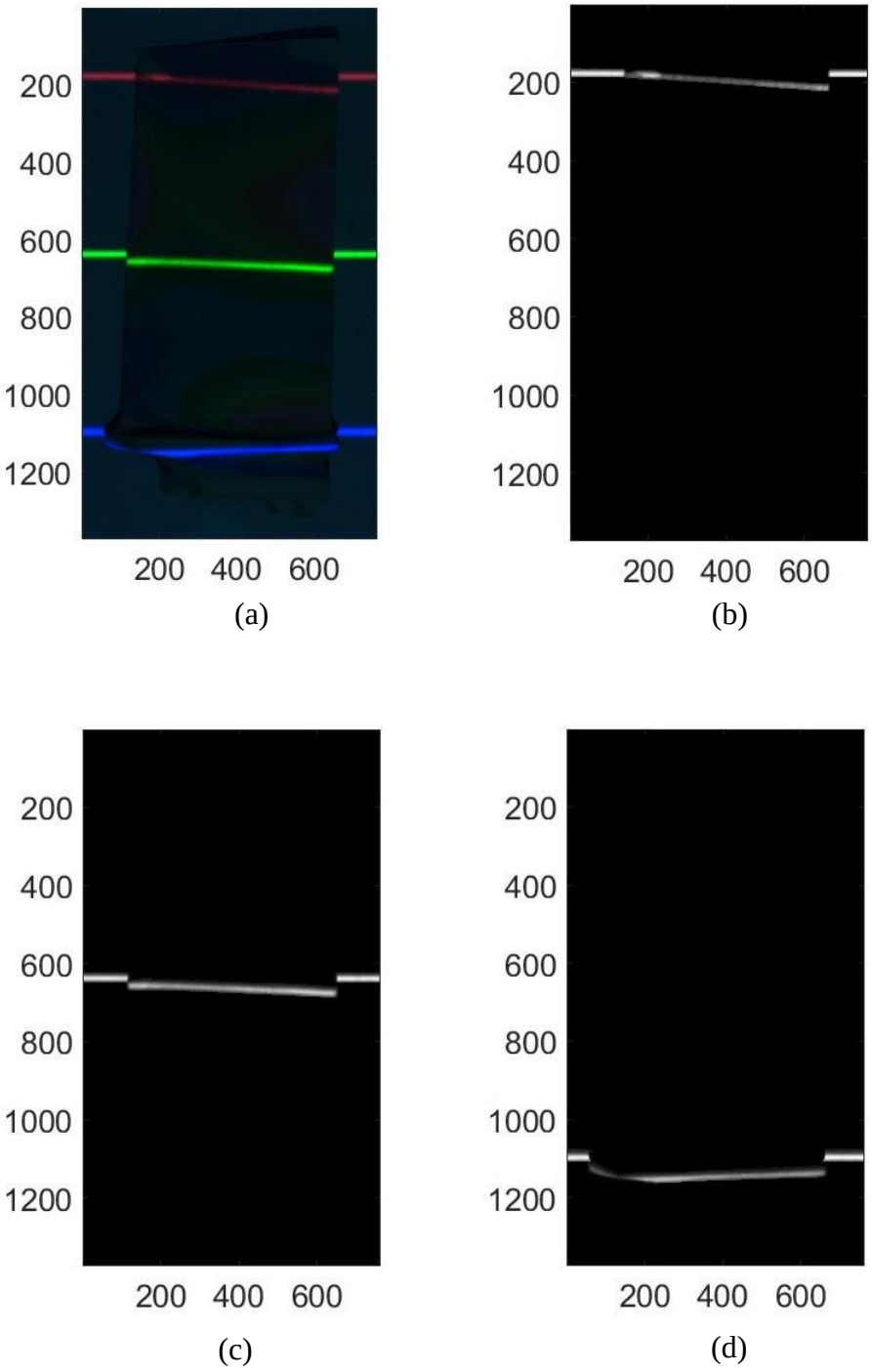

Figure 4.6. a) Typical captured image of the test object with projected color lines. **(b)**, **(c)** and **(d)** lines segmentation by color of the R, G, and B color channels in grayscale, respectively.

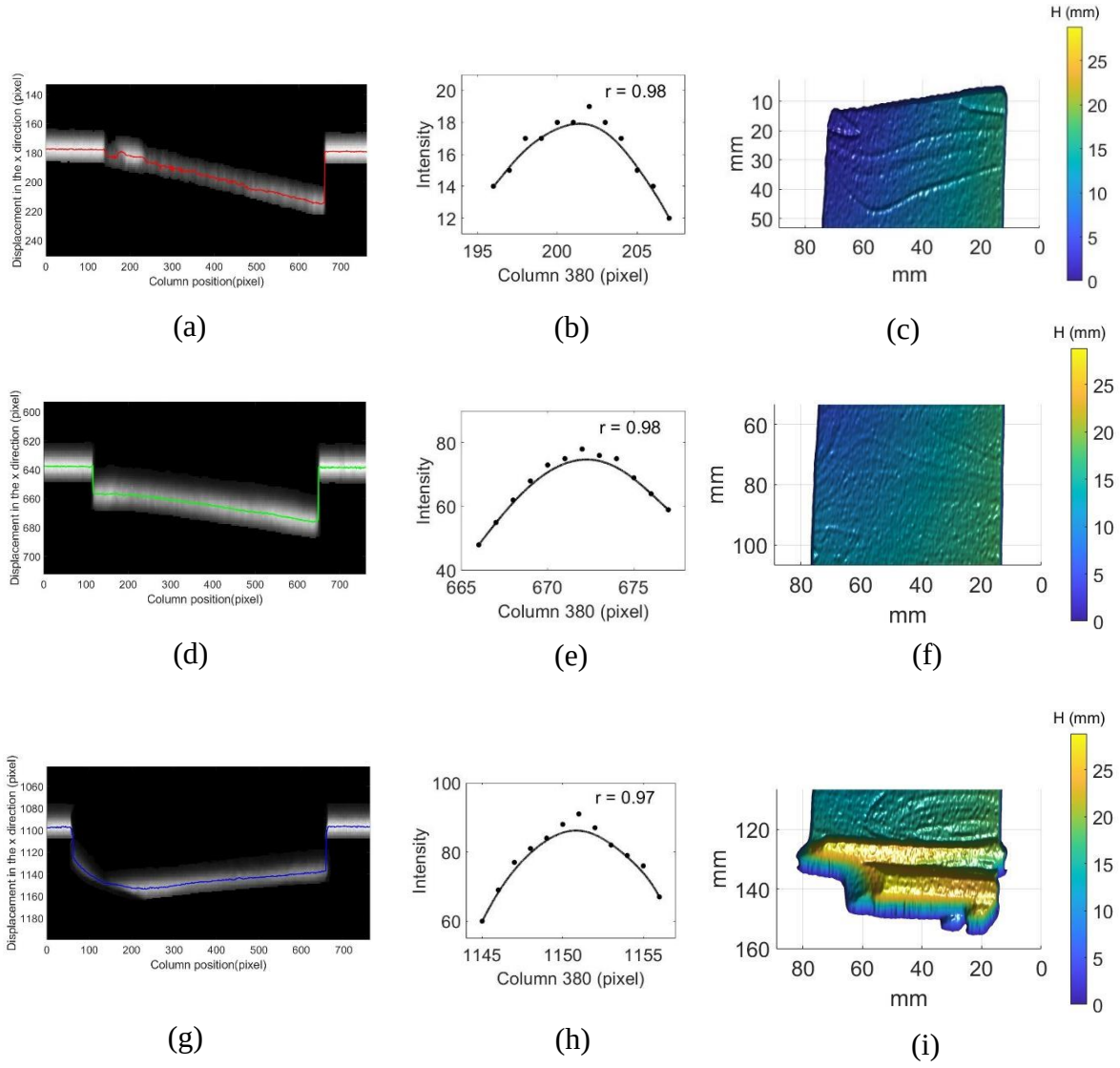

Figure 4.7. The first column shows the images of a color line in grayscale and its skeleton (red, green, and blue line) in each R, G, and B color channel; the second column shows the intensity distribution of a color line profile along column 380 (black dots) fitted to a continuous function (continuous line) in each R, G, and B color channel; and the third column shows the 3D reconstruction of the test object in each RGB color channel.

As we mentioned above, in our experiments, the projected profiles of the color lines were of the Gaussian type; hence, the skeleton was obtained by the combined Bezier curves method with the bisection method, described in section 2.1. Figs. 4.7.(a), 4.7.(d), and 4.7.(g) show the result of the skeleton obtained (red, green and blue line, respectively) of the image of Fig. 4.6.(a), in the R, G, and B channels, respectively. Figs. 4.7.(b), 4.7.(e), and 4.7.(h) show the intensity distribution of the color lines along column 380 (black dots) which fit a Bezier polynomial function (continuous line). In all cases, a correlation coefficient was obtained equal to or greater than 0.97, this value shows high confidence in the fit. It is important to note that discontinuities lines were captured, which occur due to shadows generated by the same test object or due to low illumination in some areas of this. These discontinuities can be corrected by interpolation methods which allow connecting of the broken lines to each other, as proposed in the references [59, 61]. However, if you want to correct discontinuities very large, we recommend to use the mobile configuration (between the color CCD camera and the multimedia projector) proposed in reference [79], but if a mobile configuration is dispensed with, we suggest to avoid interpolation of the occluded zone, since these algorithms will inevitably fail. The 3D shape of the test object was obtained in each color channel after calculating the skeletons of the projected lines, the results are shown in Figs. 4.7.(c), 4.7.(f), and 4.7.(i). The 3D shapes obtained in each color channel are assembled to obtain the complete 3D shape of the test object, the final result is shown in Fig. 4.8. Fig. 4.8 shows even details of the surface of the object that are not very evident to the human eye due to the color of the object, this demonstrates that our proposal also allows obtaining the 3D shape of the object with a high lateral resolution.

Through our scanning system, it was also possible to obtain the 3D shape of other types of interesting objects such as the small sculpture shown in Fig. 4.9.

In summary, the results demonstrate the efficiency of our algorithms regarding lines segmentation by color, allow us to calculate the skeletons of the color lines with sub-pixel accuracy, and allow us to obtain the 3D shape of the object with a high lateral resolution with a capture time three times faster compared to the technique of projection of one light line described in chapter 3.

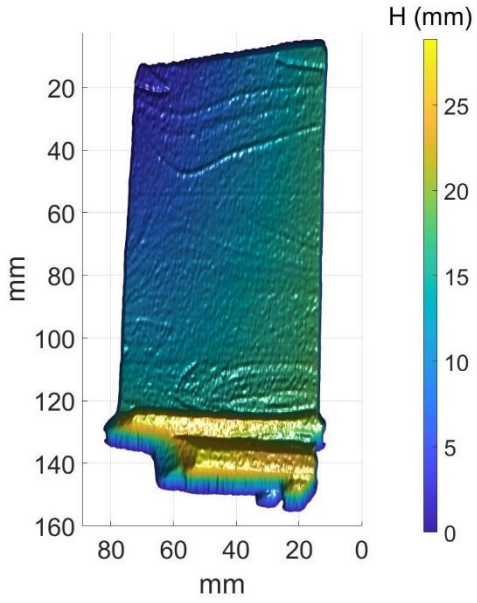

Figure 4.8. The complete 3D shape of the test object is shown.

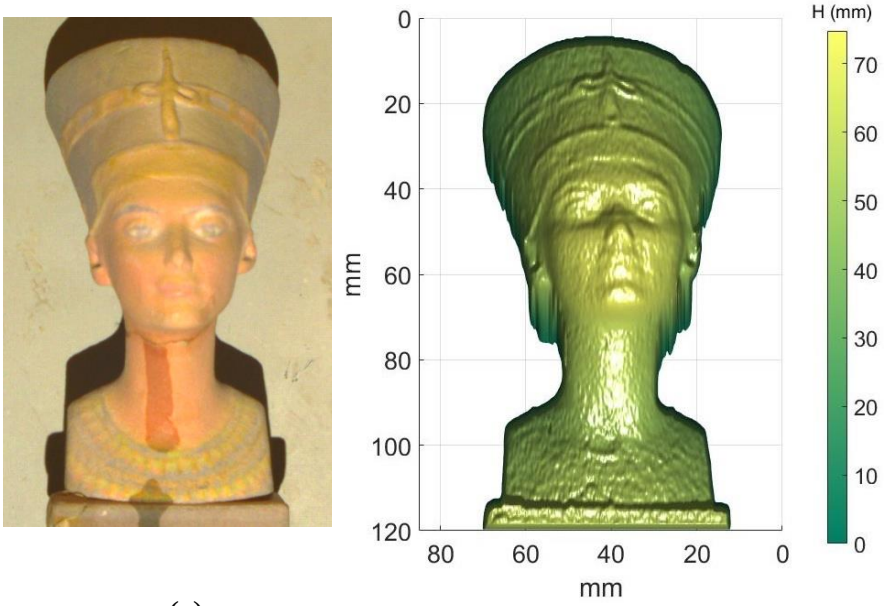

(a) (b)

Figure 4.9. (a) Image of a small sculpture to be reconstructed. **(b)** The 3D shape of the small sculpture.

4.5 CONCLUSIONS

A 3D scanning system of objects by projection of three color lines (red, green, and blue) with Gaussian profile was proposed. This proposal allows to simultaneously scan different zones of an object to be reconstructed three-dimensionally, optimizing the capture times and the number of images stored, compared to the projection of one light line. This was possible due to our proposal takes advantage of the RGB color channels of the color CCD camera. Our results show that the algorithms for lines segmentation by color implemented, which do not require threshold values, are robust to the color and reflectance of the object's surface, and ambient lighting. Besides, algorithms based on Bezier curves allowed obtaining the skeleton of color lines with sub-pixel accuracy. Along with the above, it was possible to get the shape of 3D objects with a high lateral resolution as shown in Figs. 4.8 and 4.9. Our proposal is an extension to the work carried out in chapter 3 and in reference [16].

CHAPTER 5: 3D SCANNING OF OBJECTS BY COLOR STRUCTURED MULTI-LINE PROJECTION WITH GAUSSIAN PROFILE

In this chapter, we propose an approach to obtain the 3D shape of objects through scanning by color structured multi-line projection with Gaussian profile. This proposal aims to significantly optimize the capture time and the number of images to process with respect to the methods proposed in chapters 3 and 4. The proposal consists of projecting a set of gratings with equidistant parallel lines of color red, green, and blue on the object to be reconstructed, and through image processing captured of the gratings, the displacement of the color lines is obtained by skeletonization in the R, G, and B color channels. The main challenge of image processing is to group in each color channel all the line segments belonging to each of the light lines, for this reason, a simple grouping method based on the area of the line segments was developed. Once the line segments are grouped in each color channel, the skeletonization process is carried out using the Bézier curve method described in section 2.1. The skeletons of the light lines are stored in the columns of a matrix for each color channel, later the columns of each matrix are combined to obtain the skeleton of the light lines for each captured grating. Subsequently, the displacement of the skeletons of the color lines of each grating is obtained with respect to the skeletonization of the same grating projected on a reference plane. A data matrix stores the displacements of the light lines of each grating, respectively. The 3D shape of a test object in pixel units is obtained by fusion the columns of the displacement matrices corresponding to each grating. The three-dimensional measurements of the object in units of millimeters were obtained through a previous calibration process based on the reference [10]. Our proposal allowed scanning objects with high pixel density and resolution.

5.1 EXPERIMENTAL SETUP

In Fig. 5.1, the geometric scheme composed of a multimedia projector is shown, which projects structured light lines in red (R), green (G), and blue (B) sequentially and equidistant. A CCD camera, placed perpendicular to the reference plane, captures images of the projected lines deformations caused by the shape of the surface of an object under test. According to Fig. 5.1, the reference plane is laid in the $x - y$ plane, the heights data of the object regarding the reference plane are represented by $h(x, y)$. If a single ray of a

color line is projected at point H of the object, then that same ray on the reference plane will move from point A to B. The displacement of a single ray of color is represented by $s(x, y)$. The height $h(x, y)$ at the point H on the object under test is calculated by Eq. (5.1) [14] only if the parameters D and d (related to the geometry of the optical system) are known.

$$h(x, y) = \frac{Ds(x, y)}{d + s(x, y)} \qquad (5.1)$$

The 3D shape of the object under test is obtained by calculating the displacement of all the projected color lines.

The displacements $s(x, y)$ of the color lines can be calculated by processing the captured image when the lines are projected onto the object and the captured image when the lines are projected only onto the reference plane. In both images the skeleton of the lines is calculated, and then these are stored in a data matrix for each of them, respectively. The difference of both matrices allows obtaining the displacements $s(x, y)$ in units of pixels; however, it is possible to convert these units to real units if the size of each pixel is known.

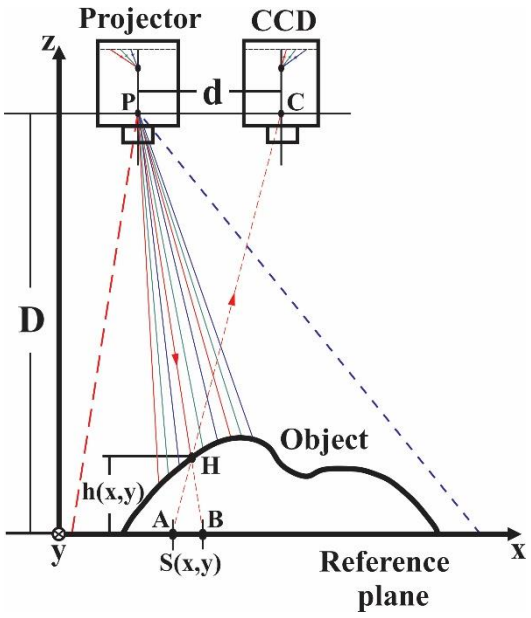

Figure 5.1. Geometry of the 3D scanning system by color structured multi-line projection.

It is important to highlight three points of the proposed approach:

- The skeletonization of the color lines is one of the main challenges to obtain the 3D shape of objects. Our proposal for this is described in detail in section 5.3.
- It is not possible to measure with accuracy the D and d parameters of our scanning system, because the manufacturing engineering of the camera and the projector does not allow knowing the positions of the pupils of both devices (points P and C in Fig. 5.1).
- The parameter D is not really a constant value because Eq. (5.1) was obtained considering that the points P, C, B, A, and H are located in the $x-z$ plane; however, the object also extends in the direction of the y-coordinate. Therefore, the parameter D is really a function of the x and y coordinates, so Eq. (5.1) is rewritten as:

$$h(x,y) = \frac{s(x,y)}{m(x,y) + n(x,y)s(x,y)} \qquad (5.2)$$

where:

$$m(x,y) = d/D(x,y) \qquad (5.3)$$

$$n(x,y) = 1/D(x,y) \qquad (5.4)$$

The coefficients $m(x,y)$ y $n(x,y)$ are related to the configuration of the optical system and whose values can be obtained by a previous calibration, which is described in detail in the section 5.6. Our calibration proposal is based on the reference [10].

5.2 COLOR STRUCTURED MULTI-LINE PROJECTION WITH GAUSSIAN PROFILE

For 3D scanning the entire surface of the object, a set of gratings (previously generated) are projected parallel to the y-axis with color multi-lines: R, G, and B,

distributed sequentially in that order, separated by black space. The gratings to be projected begins at the top with a red line and end at the bottom with a blue line, as shown in Fig. 5.2. Let us define the set of gratings as $\Psi^m = \{\Psi^1, \Psi^2, \dots, \Psi^k\}$ where m is the order in which each grating is projected and k represents the total of these.

It is necessary to consider the number of pixels between the color lines of the first projected grating in order to project the number of additional gratings that allow scanning the surface of the object over all the pixels of the region of interest.

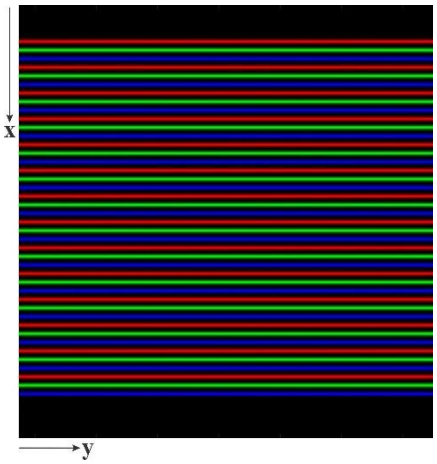

Figure 5.2. Grating of structured light with color multi-lines to project.

For example, if the first grating to be projected was generated with a separation between the color lines given by r, then have to be projected $(r - 1)$ additional gratings. These additional gratings are projected sequentially in such a way that the color lines are moved one pixel down from the color lines of the grating that was previously projected, in this way the complete scanning of the object is carried out.

Finally, for each color, the same number of lines is projected. Let us define the lines number for each color by f, i.e., the total number of lines projected is $3f$.

5.3 RECOGNITION OF STRUCTURED LIGHT LINES IN AN IMAGE

The CCD camera captures the images of the gratings projected on the object or reference plane in the RGB format of MxN pixels in size.

Since the recognition algorithms were implemented to detect vertical lines, the captured images were rotated 90° to the left, (now the size of the images is NxM). The set of captured images will be defined as $I^m = \{I^1, I^2, \dots, I^k\}$, where m is the order in which each gratings projected was captured and k represents the total of these.

Recognition of the color multi-lines of the images captured is performed independently on the R, G, and B channels in grayscale. Therefore, each captured image I^m is decomposed into a set of three images which are represented by $I^{m,ch} = \{I^{m,R}, I^{m,G}, I^{m,B}\}$.

In summary, the procedure for recognizing the color multi-lines of each images I^m, is carried out in their respective color channels represented by $I^{m,ch}$ in two stages: Segmentation of the lines, and the grouping and skeletonization of these. The two stages are described below.

5.3.1 Segmentation of the lines

This procedure aims to remove the background light from the image set $I^{m,ch}$. To perform this task, the images $I^{m,ch}$ are filtered in the frequency space by a Butterworth filter. A practical way is to obtain the background light images from the images $I^{m,ch}$ using a low-pass filter, and then subtract the background light images to the same images $I^{m,ch}$, respectively.

The design of a low-pass Butterworth filter in frequency space, of order n and with cut-off frequency D_0 from the origin is defined by the following equation [35]:

$$H(u,v) = \frac{1}{1 + \left[\frac{D(u,v)}{D_0}\right]^{2n}} \qquad (5.5)$$

where $D(u,v)$ is the distance from the point (u,v) to the origin of the frequency plane. $D(u,v)$ is calculated by the following equation:

$$D(u,v) = (u^2 + v^2)^{1/2} \qquad (5.6)$$

Subsequently, the binarization process by thresholding is carried out; however, it is possible that after this process there are broken lines (or discontinue lines) in the image $I^{m,ch}$. Broken lines significantly hinder the complexity of the grouping process of the line segments belonging to one line; for this reason, we propose the use of the morphological dilation operation [35, 36] on the binarized image in order to greatly reduce the number of discontinuous lines or at least reduce the large discontinuities between them.

The use of a suitable structural element is important in the dilation operation, since if it has small dimensions, the effect on the broken lines will be minimal; on the contrary, if it has very large dimensions, the lines will overlap each other. At this point, the importance of our proposal to project color multi-lines becomes evident since it aims to achieve a large distance between lines of the same color and thus ensure that the use of a relatively large structural element does not cause the lines to overlap each other.

Finally, after the dilation operation, the set of segmented images of the images $I^{m,ch}$ is obtained which is represented by $Mask^{m,ch}$. In general, $Mask^{m,ch}$ is called the mask of $I^{m,ch}$.

5.3.2 Grouping and skeletonization of light lines

The light lines of the images $I^{m,ch}$ do not present the problem of broken lines when the set of gratings is projected on the reference plane. On the contrary, when the projection is made on an object with abrupt variations in its surface, the lines of the images $I^{m,ch}$ almost always present discontinuities. For this reason, it is fundamental that we can identify the line segments that belong to one line in each image $I^{m,ch}$ since if a line segment is mistakenly connected to any neighboring line, it will produce a false 3D reconstruction. The dilation operation allows the broken lines to be greatly reduced; however, this procedure does not completely solve the problem when the discontinuities are very large. We propose a simple grouping algorithm based on the areas of the line segments of each image $I^{m,ch}$ (whose respective masks are $Mask^{m,ch}$). Once one line is grouped with its respective line segments, the skeletonization process proceeds. The grouping and skeletonization process is repeated until the last line of each image $I^{m,ch}$.

Our proposal consists of projecting light lines whose condition is that the lines projected on the reference plane are much longer than those that are projected onto the object, as shown in the diagram of Fig. 5.3.(a) (where line segments of the same color belong to the same line). When an object placed on a reference plane is illuminated by the grating, the section of the lines of the grating projected on the plane are continuous, while the section projected on the object may be discontinuous. Therefore, based on the condition mentioned above, if a projected line is broken, the longest line segment will be projected onto the reference plane and the shortest line segments will be projected onto the object. To ensure the correct performance of our proposal, the object must be in the center of the field of view, the projected lines should not overlap each other, and the last line of the masks $Mask^{m,ch}$ must be continuous.

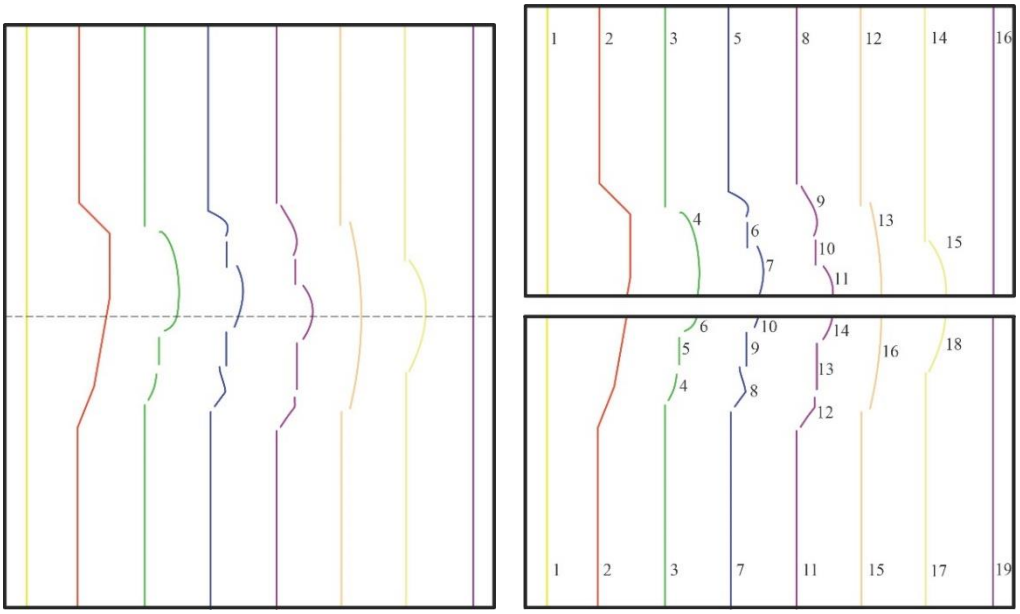

(a) (b)

Figure 5.3. (a) Representation of the image line segments of a mask $Mask^{m,ch}$. **(b)** Illustration of the labeling of the line segments of the masks $Mask_{up}^{m,ch}$ and $Mask_{low}^{m,ch}$.

Prior to the grouping and skeletonization process, the images $I^{m,ch}$ are divided into two halves, upper $I_{up}^{m,ch}$ and lower $I_{low}^{m,ch}$. In the same way, the masks $Mask^{m,ch}$, upper $Mask_{up}^{m,ch}$ and lower $Mask_{low}^{m,ch}$. Therefore, any of the images $I_{up}^{m,ch}$ (or $I_{low}^{m,ch}$), it has its respective mask $Mask_{up}^{m,ch}$ (or $Mask_{low}^{m,ch}$).

Below we will detail the steps of the grouping process:

Step 1. Labeling of the segments of the light lines. The procedure for labeling line segments of the images $Mask_{up}^{m,ch}$ is carried out through the algorithm proposed by Haralick et al [80]. This algorithm, implemented in MATLAB, labels the components (in our case, the line segments) of an image in way consecutive, starting the search for each component in the direction from top to bottom in each column of the image. This procedure obtains a labeled image L for each mask $Mask_{up}^{m,ch}$. To each line segment of the labeled images L is assigned its own unique label i, where $i = 1, 2, \dots, n$, and n is the total number of line segments. An illustration of the labeling of the line segments of the masks $Mask_{up}^{m,ch}$ and $Mask_{low}^{m,ch}$ is shown in Fig. 5.3.(b).

Step 2. A threshold area T_A is declared. The grouping of the line segments is based on the condition of a threshold area T_A, which according to experience, is calculated as 40% of the line segment with the largest area. Line segments projected onto the reference plane are always greater than T_A.

Step 3. Grouping process of the line segments belonging to one line of the masks $Mask_{up}^{m,ch}$. The binary images C and $Mask_{line}$ with pixel values equal to 0 are created. C and $Mask_{line}$ have the same dimensions as $Mask_{up}^{m,ch}$. The image C will store one line segment belonging to the label i of the labeled images L of any of the masks $Mask_{up}^{m,ch}$, while the image $Mask_{line}$ will accumulate all the line segments that belong to the same light line (in other words, $Mask_{line}$ is the mask of one light line). Suppose all the indexes in the vertical direction of the captured image form the set, $X = \{1, 2, \dots, N\}$ and all the indexes in the horizontal direction form the set, $Y = \{1, 2, \dots, M\}$. For any of the masks $Mask_{up}^{m,ch}$, the grouping process begins by obtaining the set of positions $(\bar{X}, \bar{Y})$ of the respective labeled image L whose pixels belong to the label i, that is:

$$(\bar{X}, \bar{Y}) = \{(x, y)/x \in X, y \in Y, L(x, y) = i\} \quad (5.7)$$

Then, the values of the positions $(\bar{X}, \bar{Y})$ of the image C are assigned to 1, that is:

$$C(x, y) = 1, \qquad \forall (x, y) \in (\bar{X}, \bar{Y}) \quad (5.8)$$

C is assigned to $Mask_{line}$, i.e.:

$$Mask_{line}(x, y) = C(x, y) \quad (5.9)$$

Next, C is updated assigning the value of 0 to all the pixels.

Coming up next, the area of the subsequent line segment to i whose label is j (where $j = i + 1$, and A_j represents the area of label j), is compared to T_A. At this point, two conditions can occur:

- **Condition 1: $A_j \leq T_A$.** If this condition is met, then the line segments with labels i and j belong to the same line, therefore the line segments of the mask $Mask_{up}^{m,ch}$ which corresponds to labels j of the labeled image L, is assigned to the accumulator image $Mask_{line}$. For this, by means of Eq. (5.7), the set of positions $(\bar{X}, \bar{Y})$ of the pixels now belonging to the label j are obtained, and by means of Eq. (5.8), the value of 1 is assigned to the set of positions $(\bar{X}, \bar{Y})$ of the image C. Finally, the image C is assigned to the accumulator image $Mask_{line}$, this is:

  $$Mask_{line}(x, y) = Mask_{line}(x, y) + C(x, y) \quad (5.10)$$

  Again, C is updated assigning the value of 0 to all the pixels. The value of j is updated by increasing its value by one unit, i.e., $j = j + 1$.

  The area of the line segment of label j (updated value of j) is again compared with T_A, and the process is repeated until the area of some line segment

corresponding to the label j is greater than T_A ($A_j \geq T_A$). When this happens, the value of i is update making $i = j$.

- **Condition 2: $A_j \geq T_A$.** If this condition is met, then the line segments with labels i and j belong to different lines. In this case, the value of i is update making $i = i + 1$.

After any of the conditions have been met, the mask of one line (represented by $Mask_{line}$) will have been formed by the grouping of one or more line segments. The line to be skeletonized is obtained by multiplying pixel by pixel between the image of $Mask_{line}$ and its respective image $I_{up}^{m,ch}$, this is:

$$I_{up}(x, y) = I_{up}^{m,ch}(x, y) Mask_{line}(x, y) \qquad (5.11)$$

where $I_{up}(x, y)$ represents the image of the line in question whose skeleton will be obtained next.

Step 4. Skeletonization of one light line. This procedure is carried out by the Bézier polynomial method, which is described in detail in the section 2.1 and is based on the references [14, 16, 68]. The procedure allows obtaining the skeleton positions with sub-pixel resolution of the image I_{up}, and whose values are stored consecutively in the columns of the data matrix which is represented by $P_{up}^{m,ch}$; the indices m, ch, and up have been defined previously. $P_{up}^{m,ch}$ stores the skeleton positions of the lines belonging to image $I_{up}^{m,ch}$. It is important to note that the size of the matrix $P_{up}^{m,ch}$ is $(N/2)x(f)$, remembering that N is the number of pixels in the vertical direction of the image, and f is the number of lines projected and captured in each color channel.

Step 5. Updated of the images $Mask_{line}$ and I_{up} assigning the value of 0 to all their pixels.

Step 6. Repetition of the steps 3 to 5 until the line segment with label $i = n - 1$ of the respective labeled image L.

Step 7. Skeletonization of the last line with label $i = n$. As we mentioned earlier, the last line has to be continuous, that is, it is formed of a single line

segment; therefore, the area of the line in question will always be greater than T_A. The skeleton positions of the last line are stored in column f of the respective matrix $P_{up}^{m,ch}$.

Step 8. Steps 1 to 7 are repeated, but now to get the grouping of all the line segments belonging to the masks $Mask_{low}^{m,ch}$ and get the skeleton positions represented by $P_{low}^{m,ch}$ of the respective images $I_{low}^{m,ch}$.

Step 9. Concatenation of matrices $P_{up}^{m,ch}$ and $P_{low}^{m,ch}$. In this step, finally, the positions of the skeleton for any of the processed images $I^{m,ch}$ are stored in the set of matrices represented by $P^{m,ch} = \{P^{m,R}, P^{m,G}, P^{m,B}\}$. The set of matrices $P^{m,ch}$ is obtained by:

$$P^{m,ch} = \begin{bmatrix} P_{up}^{m,ch} & P_{low}^{m,ch} \end{bmatrix}^T \qquad (5.12)$$

remembering that m represents any of the captured images, ch represents the respective color channel, and $[\,.\,]^T$ indicates the transpose of the matrix.

5.4 OBTAINING THE 3D SHAPE OF OBJECTS WITH LOW-RESOLUTION

The procedure to obtain the shape of the object with low-resolution is based on calculating the displacement of the skeletons of any of the captured images I^m of the gratings projected onto an object with respect to the same grating projected onto the reference plane.

The skeletons positions of any image I^m are stored in the columns of the data matrix that we will represent by E^m (it is clear that E^m has $3xf$ columns). The matrix E^m is computed by the appropriate combination of the columns of the matrices $P^{m,R}$, $P^{m,G}$ and $P^{m,B}$ obtained by Eq. (5.12) and that are represented by $P^{m,ch}$. The combination of the columns is linked to the respective color lines of the image I^m. The matrix E^m, for any of the images I^m, is structured as follows:

$$E^m = \begin{bmatrix} P_1^{m,R} & P_1^{m,G} & P_1^{m,B} & \cdots & P_f^{m,R} & P_f^{m,G} & P_f^{m,B} \end{bmatrix} \qquad (5.13)$$

where the sub-indices indicate the positions of the columns of the respective matrices $P^{m,R}$, $P^{m,G}$ and $P^{m,B}$.

In parallel, in the same way, a matrix $E^{m\prime}$ that stores the skeletons positions of the captured images of the light lines projected on the reference plane is determined.

The displacement of the lines of any of the images I^m is calculated in a simple way by the difference between the matrices E^m and $E^{m\prime}$, this is:

$$s^m(x,y) = E^m - E^{m\prime} \qquad (5.14)$$

The results obtained by this approach are comparable with references [25, 26, 31, 33], and whose results will be shown in section 5.8.2.

5.5 OBTAINING THE 3D SHAPE OF OBJECTS WITH HIGH PIXEL DENSITY

So far, our scanning system has captured a set of images, which scan all the pixels projected on the area of interest where the object is located. The captured images were rotated 90° to the left, these were defined by I^m where $I^m = \{I^1, I^2, \dots, I^k\}$. The color lines of each image I^m have been skeletonized; the set of matrices containing the positions of the skeleton of each image I^m was defined by E^m where $E^m = \{E^1, E^2, \dots, E^k\}$. To get the 3D shape of the object with high pixel density, it is necessary to obtain the skeleton of all the lines projected on the area of interest, this task is carried out in a simple way by combining the columns of the set of matrices E^m. The way in which the scanning is carried out on the area of interest is as follows: The first k columns of the area of interest are scanned by the first line (red) of the gratings in the order they were projected, the next k columns are scanned by the second line (green) of the projected gratings and so on until the last k columns are scanned by the last line (blue) of the projected gratings; therefore, it is evident that the matrix that contains the positions of the skeleton of all the lines projected on the object is obtained by combining the columns whose structure is the following:

$$T = \begin{bmatrix} E_1^1 & E_1^2 & \cdots & E_1^k & E_2^1 & E_2^2 & \cdots & E_2^k & \cdots & E_{3xf}^1 & E_{3xf}^2 & \cdots & E_{3xf}^k \end{bmatrix} \quad (5.15)$$

where the sub-indices indicate the positions of the columns of the respective matrices belonging to the set $E^m = \{E^1,\ E^2, \ldots, E^k\}$.

In parallel, in the same way a matrix is calculated, which we will define by T', which contains the skeleton positions of all the lines projected on the reference plane.

Finally, the displacement of all the light lines projected on the area of interest where the object is located is calculated in a simple way by:

$$s(x, y) = T - T' \quad (5.16)$$

The calculation of the matrix $s(x, y)$ allows obtaining the 3D shape of objects in units of pixels. Object dimensions in units of lengths are obtained through a calibration process described in the next section.

5.6 EXPERIMENTAL OBTAINING OF THREE-DIMENSIONAL MEASUREMENTS IN REAL COORDINATES

In section 5.1, it was mentioned that, due to the manufacture of the camera and projector, it is not possible to accurately measure the parameters D and d of our optical system (see Fig. 5.1); furthermore, the parameter D depends on the x and y coordinates. For this reason, a calibration procedure is necessary that allows us to directly relate the displacements $s(x, y)$ of the color lines projected on the object and the heights $h(x, y)$ of the object with respect to the reference plane, without need to directly measure the parameters D and d.

Fig. 5.4 shows the scheme of the calibration system, to determine the coefficients $m(x, y)$ and $n(x, y)$ from the Eq. (5.3) and Eq. (5.4), respectively. A reference plane is placed to known distances h_i (where $i = 1, 2, \ldots Z$, and Z is the number of positions) regarding the position $z = 0$ of the reference plane. The height for each point (x, y) of the reference plane at each calibration position is calculated by:

$$h_i(x,y) = \frac{s_i(x,y)}{m(x,y) + n(x,y)s_i(x,y)} \qquad (5.17)$$

where $s_i(x,y)$ are the displacements of each pixel of the skeleton of each line in the position h_i of the reference plane regarding the position $z = 0$. The calculation of $s_i(x,y)$ is obtained using the methodology described in section 5.5.

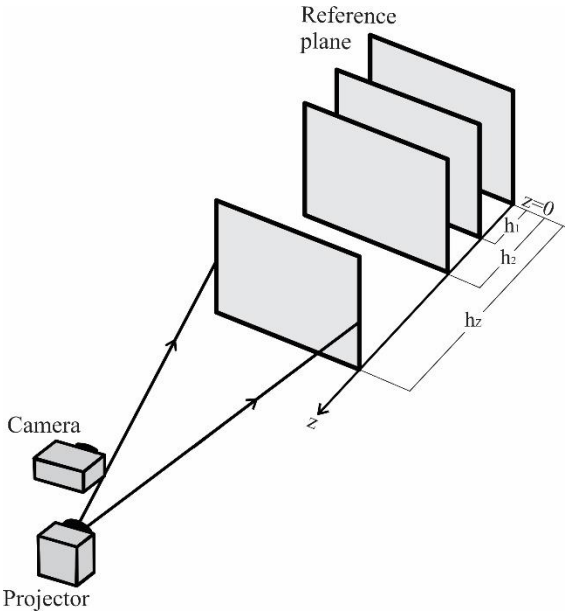

Figure 5.4. Schematic of the 3D scanning system for calibration.

In our case, following a procedure analogous to reference [10], which is based on the least-squares method, the parameters $m(x,y)$ and $n(x,y)$ are calculated directly by the following equations:

$$m(x,y) = \frac{a_3(x,y)b_1(x,y) - a_2(x,y)b_2(x,y)}{a_1(x,y)a_3(x,y) - a_2^2(x,y)} \qquad (5.18)$$

$$n(x,y) = \frac{a_1(x,y)b_2(x,y) - a_2(x,y)b_1(x,y)}{a_1(x,y)a_3(x,y) - a_2^2(x,y)} \qquad (5.19)$$

where:

$$a_1(x,y) = \sum_{i=1}^{Z} h_i^2(x,y) \qquad (5.20)$$

$$a_2(x,y) = \sum_{i=1}^{Z} h_i^2(x,y)s_i(x,y) \qquad (5.21)$$

$$a_3(x,y) = \sum_{i=1}^{Z} h_i^2(x,y)s_i^2(x,y) \qquad (5.22)$$

$$b_1(x,y) = \sum_{i=1}^{Z} h_i(x,y)s_i(x,y) \qquad (5.23)$$

$$b_2(x,y) = \sum_{i=1}^{Z} h_i(x,y)s_i^2(x,y) \qquad (5.24)$$

Finally, when the coefficients $m(x,y)$ and $n(x,y)$ have been determined, the 3D real coordinates of the surface of an object can be calculated directly by Eq. (5.2).

5.7 EXPERIMENTAL PART

The diagram in Fig. 5.5.(a) shows the 3D scanning system by color multi-line projection. The multimedia projector (resolution of 1280x800 pixels) projects images at an oblique angle to the reference plane, while a CCD camera (resolution of 2048x1536 pixels) mounted perpendicular to the reference plane captures and digitizes the images from the color multi-lines as they move in one-pixel steps across the surface of interest

where the object is located. Remember that due to the operation of the implemented algorithms, the image will later be rotated 90°, therefore the size of the images that will be processed is 1536x2048. A computer (processor i7-3630QM of 2.40GHz, 64-bit operating system, and RAM memory of 8.0 GB) synchronizes the projection and capture of the images at a frequency of 30 fps.

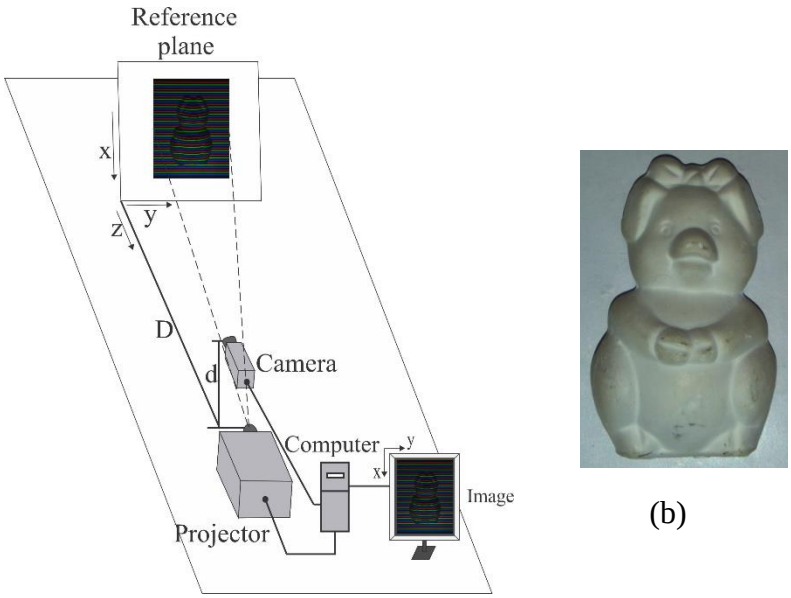

Figure 5.5. (a) Experimental setup scheme of the 3D scanning system by color multi-line projection. **(b)** Test object.

Based on section 5.2, 14 gratings to be projected were generated, represented by Ψ^m (where $m = 1, 2, \ldots 14$). Each grating Ψ^m contains 39 color lines of Gaussian profile, so the number of lines for each color is $f = 13$. The separation between the maximum intensity of the color lines was $r = 14$ pixels. The color lines of the gratings from Ψ^2 to Ψ^{14} are moved $(m - 1)$ pixels from top to bottom with respect to the grating Ψ^1, which allowed scanning all the projected pixels of the surface of interest. Fig. 5.2 shows one of the images (Ψ^1) to be projected. It is important to mention that the large separation between the lines of the same color ensures the correct performance of the segmentation process and consequently facilitates the grouping of the lines. Our scanning system captured the 14 projected gratings at a time of 0.47 s.

As mentioned in previous chapters, the resolution along the light line is determined by the pixel size in units of millimeters. According to Fig. 5.6, it was

determined that the width of the image is 254.0 mm which is equivalent to 2048 pixels; therefore, the lateral resolution along the light line is 0.124 mm.

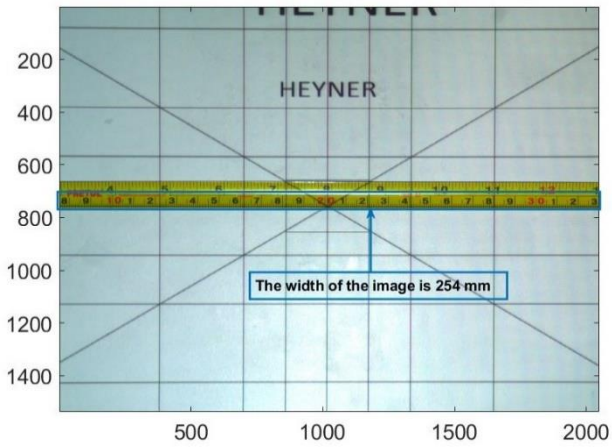

Figure 5.6. Measurement of the pixel size to obtain the resolution along the light line.

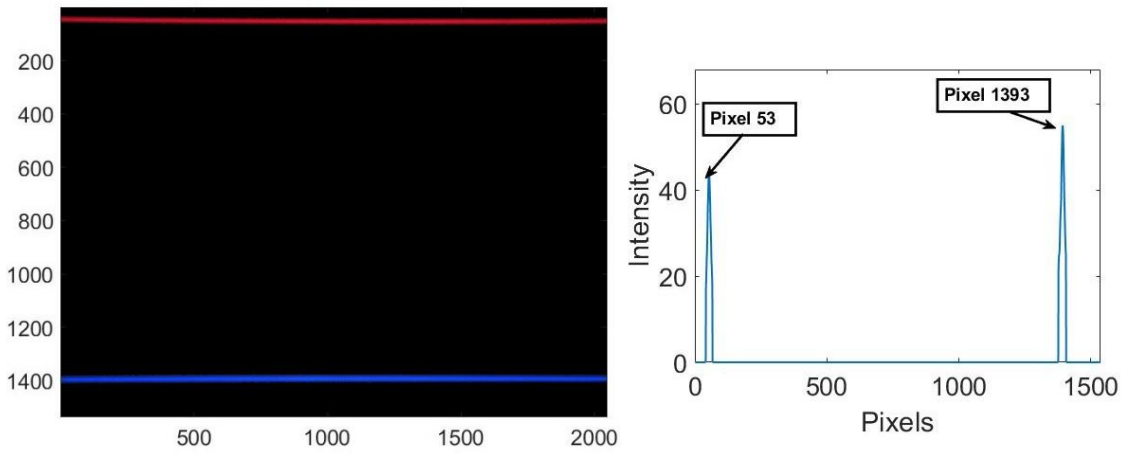

(a) (b)

Figure 5.7. (a) Result of the superposition of the upper red line of the captured image of the grating Ψ^1, and lower blue line of the captured image of the grating Ψ^{14}. **(b)** Positions in pixels of the maximum intensity of the red light line and blue light line.

To obtain the resolution in the transverse direction of the light line, was measured the number of pixels between the first upper light line (red line) of the captured image of the grating Ψ^1 and the last lower light line (blue line) of the captured image captured of the grating Ψ^{14} projected on the reference plane. Fig. 5.7.(a) shows the result of the superposition of the light lines mentioned above. The upper light line corresponds to the position of the light line of the captured image of the grating Ψ^1, and the lower light line corresponds to the position of the light line of the captured image of the grating Ψ^{14}. Fig. 5.7.(b) shows the positions in pixels of the maximum intensity of the light lines in question. A total of 546 light lines were projected (each of the 14 gratings contained 39 light lines), therefore the number of steps between the light lines in question was 545 equivalents to 1339 pixels. With these known values, the resolution in the transverse direction of the light line is obtained by Eq. (3.1); this resolution was 0.305 mm.

5.8 RESULTS AND DISCUSSION

Next, we will show and comment on the results obtained from our proposal for 3D scanning objects by projection of color multi-lines.

5.8.1 Results of image processing

In the experiments carried out, our system captured a set of 14 images of the gratings projected represented by $I^m = \{I^1,\ I^2, \ldots, I^{14}\}$, in a time of 0.47 s. It is important to note that if the technique of projection of one light line, by laser [14, 68] (or multimedia projector as a source [16]), had been used in the scanning, it would have been necessary to capture a set of 546 images, which would have taken a capture time of 18.2 s. Our proposal considerably reduces the capture time by almost 40 times compared to scanning by the projection of one light line. The main advantage of this short time of capture is that it allows the application of the technique to be extended to objects that require a fast scanning due to they are susceptible to moving or changing their shape.

After capturing the set of images I^m, the procedure of recognition of color multi-lines described in section 5.3 is carried out. As mentioned, according to the working of the programmed algorithms, the set of images I^m were rotated 90° to the left in such a way that the color lines are in a vertical position, starting from the left with the red line and ending with the blue line, as shown in Fig. 5.8.(a).

The image processing is carried out on all the images I^m and the images of their respective color channels $I^{m,ch}$; however, below we will show the results for the first image captured I^1 and its color channels $I^{1,ch} = \{I^{1,R}, I^{1,G}, I^{1,B}\}$. Figs. 5.8, shows the captured image I^1 and the result of its decomposition in each channel $I^{1,R}$, $I^{1,G}$, and $I^{1,B}$, respectively.

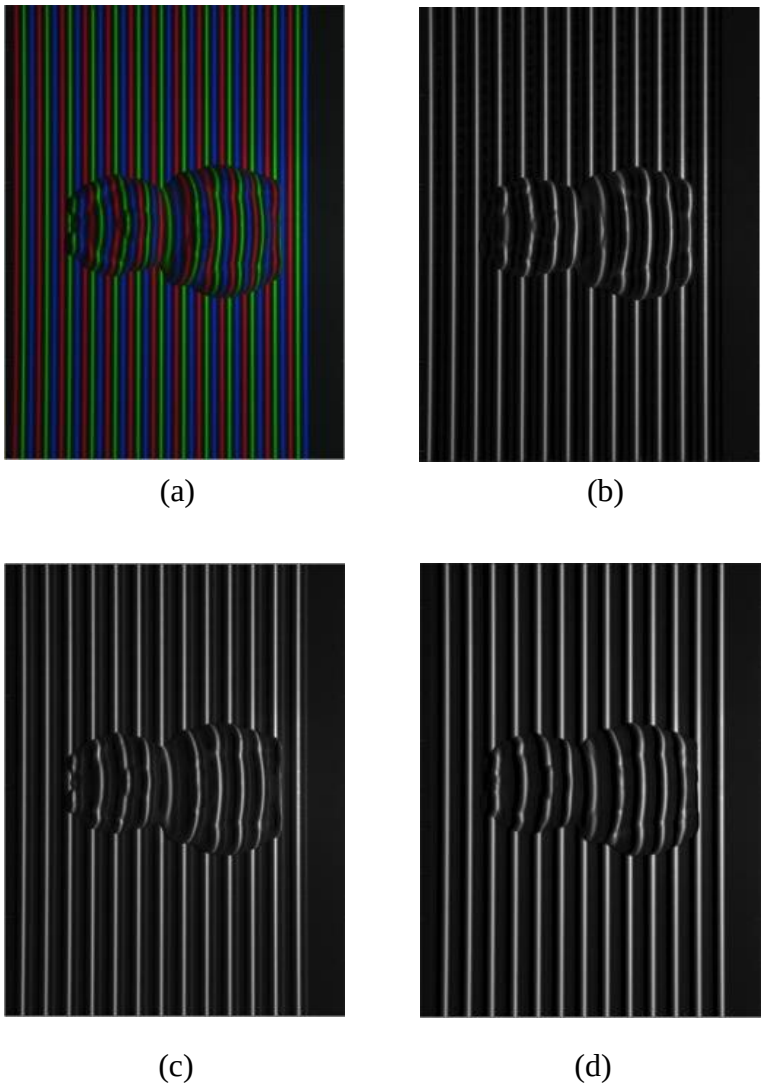

(a) (b)

(c) (d)

Figure 5.8. (a) Captured RGB image of the first projected grating and its decomposition into the color channels **(b)** red, **(c)** green, and **(d)** blue.

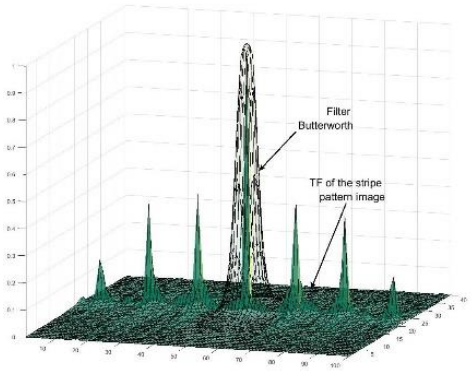

(a)

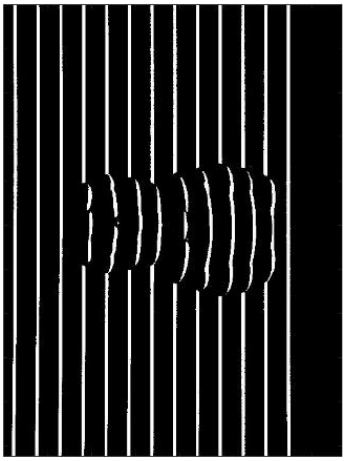

(b)

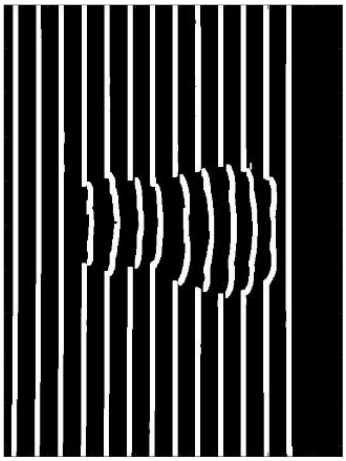

(c)

Figure 5.9. (a) Butterworth filter applied in frequency space on the R channel image. **(b)** Binarized image. **(c)** Obtaining the R channel mask after applying the morphological operation of dilation.

Afterward, the set of images $I^{m,ch}$ were filtered by a low-pass Butterworth filter in the frequency space to remove the background light. According to Eqs. (5.5) and (5.6), we design the Butterworth filter of order $n = 2$ and a cutoff frequency $D_0 = 3$. The Butterworth filter allowed to eliminate largely the background light of the images. Then, the binarization process was carried out with a threshold value greater than or equal to 50 on the grayscale. According to our proposal, to reduce the number of broken lines and the distances between

them, the morphological operation of dilation was applied with a rectangular structural element of size 30x10 pixels. This task was carried out efficiently since it was possible to use a large structural element in each color channel due to the large distances between the lines of the same color and the shape of the object. After the dilatation operation, the masks, defined by $Mask^{m,ch}$, of the images $I^{m,ch}$ were obtained. Fig. 5.9.(a) shows the result of the Butterworth filter design in the frequency space applied to the central lobe of the image $I^{1,R}$. Fig. 5.9.(b) shows the result of the binarization on the image, the presence of broken lines is observed especially around the edges of the object. In Fig. 5.9.(c), the efficiency of the dilation operation on the image is clearly observed.

One of the main challenges of our proposal is to correctly group the line segments of the masks $Mask^{m,ch}$ belonging to one light line, and then carry out the skeletonization process of the grouped line in question. The images $I^{m,ch}$ are divided into two halves $I_{up}^{m,ch}$ and $I_{low}^{m,ch}$, whose respective masks are $Mask_{up}^{m,ch}$ and $Mask_{low}^{m,ch}$. Then we proceed with the labeling of each segment of $Mask_{up}^{m,ch}$ and $Mask_{low}^{m,ch}$ by the algorithm proposed by Haralick et al [80]. Through the grouping and skeletonization described in section 5.3.2, we obtained the matrices $P_{up}^{m,ch}$ and $P_{low}^{m,ch}$ which contain the positions of the skeletons of the lines of the images $I_{up}^{m,ch}$ and $I_{low}^{m,ch}$, respectively. Finally, by concatenating both matrices using the Eq. (5.12), the matrix of positions of the skeleton $P^{m,ch}$ of the images $I^{m,ch}$ are obtained, respectively.

For example, for the case of the image $I^{1,R}$, divided into two halves $I_{up}^{1,R}$ and $I_{low}^{1,R}$ with their respective masks $Mask_{up}^{1,R}$ and $Mask_{low}^{1,R}$, the results of the labeling of the masks are shown in Figs. 5.10.(a) and 5.10.(b), respectively, where the lines present a useful pseudo color to differentiate the labels. Coincidentally, both masks present 18 line segments which were grouped and skeletonized. Figs. 5.10.(c) and 5.10.(d) show the skeletonization (red line) of the images $I_{up}^{1,R}$ and $I_{low}^{1,R}$, whose matrices of the skeleton positions are $P_{up}^{1,R}$ and $P_{low}^{1,R}$, respectively. Fig. 5.10.(e) shows the result of skeletonization (red line) of the image $I^{1,R}$, whose skeleton positions are stored in the matrix represented by $P^{1,R}$. Figs. 5.11.(a) and 5.11.(b) show also the results of the grouping and skeletonization for the images

$I^{1,G}$ and $I^{1,B}$. In this case, the positions of the skeletons were stored in the matrices $P^{1,G}$ and $P^{1,B}$, respectively.

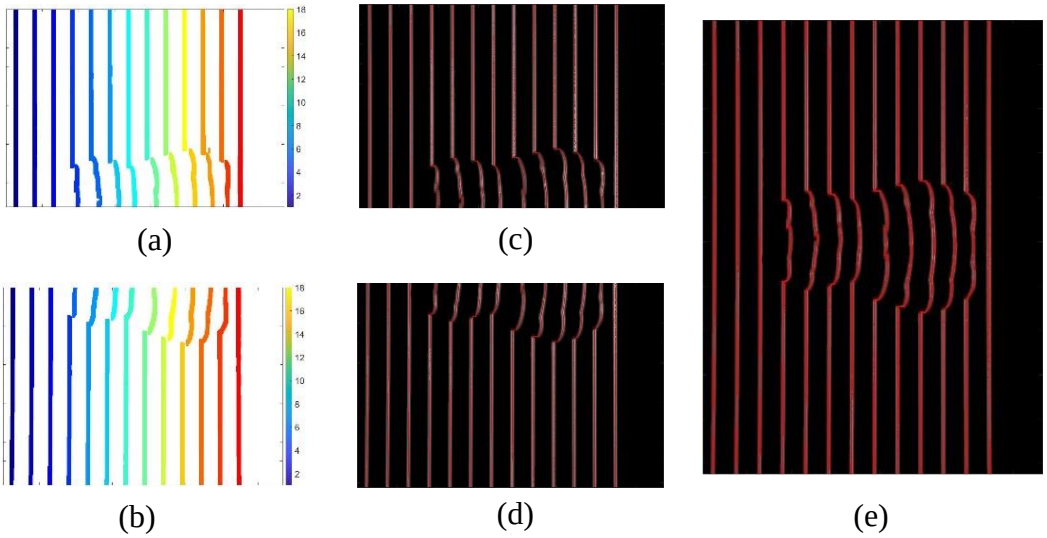

(a) (c)

(b) (d) (e)

Figure 5.10. (a), **(b)** Labeled images from $Mask_{up}^{1,R}$ and $Mask_{low}^{1,R}$. **(c), (d)** Grouping and skeletonization of lines from $I_{up}^{1,R}$ and $I_{low}^{1,R}$. **(e)** Skeletonization of lines from $I^{1,R}$.

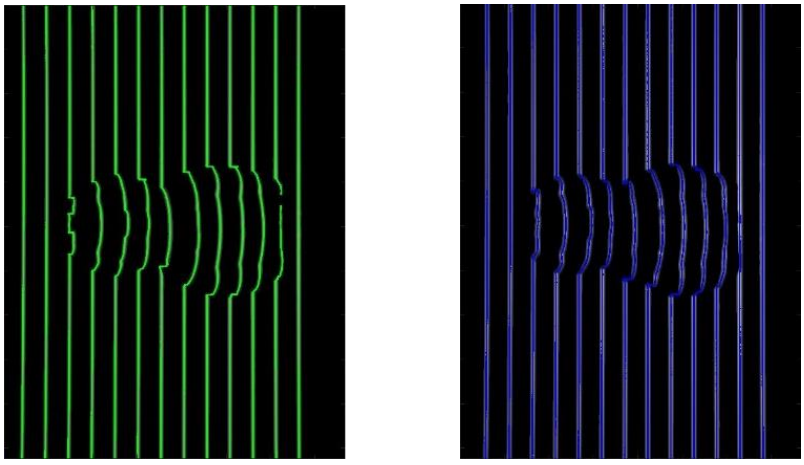

(a) (b)

Figure 5.11. (a) and **(b)** Skeletonization of lines from $I^{1,G}$ and $I^{1,B}$, respectively.

5.8.2 Results of obtaining the 3D shape of objects

The 3D shape with low-resolution is obtained by displacement of the skeleton of the color lines of any of the images I^m; however, we will show the results for the image I^1. In the previous section, the positions of the skeleton of the images in each color channel were obtained, which were stored in the matrices $P^{1,R}$, $P^{1,G}$ and $P^{1,B}$, respectively. For this case, skeletonization of image I^1 is obtained by calculating the respective matrix E^1 through the structure of Eq. (5.13), that is:

$$E^1 = \begin{bmatrix} P_1^{1,R} & P_1^{1,G} & P_1^{1,B} & \cdots & P_{13}^{1,R} & P_{13}^{1,G} & P_{13}^{1,B} \end{bmatrix} \qquad (5.25)$$

where the matrix E^1 has 39 columns, and remembering that the sub-indices indicate the positions of the columns of the matrices $P^{m,R}$, $P^{m,G}$ and $P^{m,B}$. Eq. (5.25) contains the skeleton positions of the light lines of the image I^1; Fig. 5.12.(a) shows the result, where the white lines represent the skeleton of the color multi-lines.

The same procedure is carried out to calculate the matrix $E^{1\prime}$ that contains the skeleton positions of the light lines projected on the reference plane.

According to Ec. (5.14), for the case of the image I^1, the displacement $s^1(x, y)$ is obtained by the difference between the matrices E^1 and $E^{1\prime}$, this is:

$$s^1(x, y) = E^1 - E^{1\prime} \qquad (5.26)$$

The 3D shape of the object with low-resolution obtained by Eq. (5.26) is shown in Fig. 5.12.(b) where the reconstruction of the reference plane is omitted in the figure. It is important to mention that these results are comparable to those obtained in the references [25, 26, 31, 33].

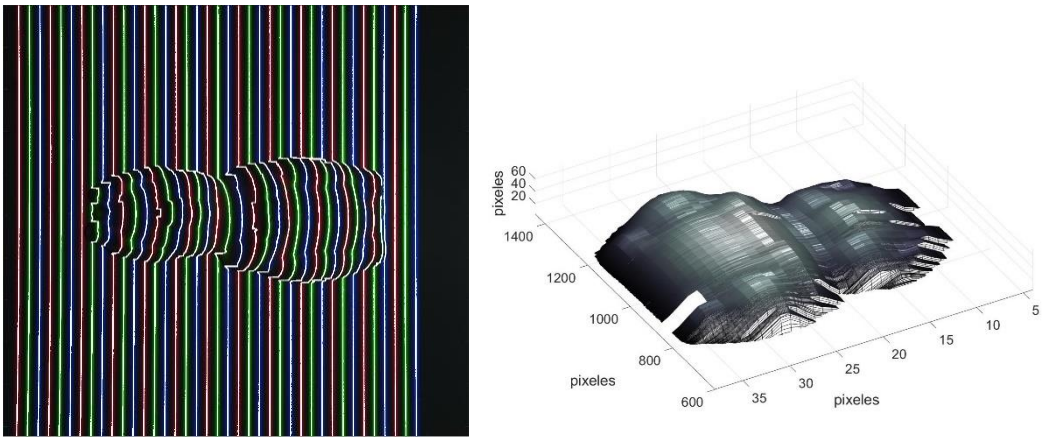

(a) (b)

Figure 5.12. (a) Complete skeletonization of the color lines of the captured image I^1. **(b)** 3D shape of the test object with low-resolution.

To obtain the 3D shape of the test object with high pixel density, the set of matrices E^m of the set of images I^m was calculated. Subsequently, the matrix T, which contains the skeleton of all the light lines projected on the object, is obtained through of the combination of the columns of E^m according to the structure of Eq. (5.15), for our experiment this is:

$$T = [E_1^1 \quad E_1^2 \quad \cdots \quad E_1^{14} \quad E_2^1 \quad E_2^2 \quad \cdots \quad E_2^{14} \quad \cdots \quad E_{39}^1 \quad E_{39}^2 \quad \cdots \quad E_{39}^{14}] \tag{5.27}$$

where the matrix T has 546 columns.

To obtain the matrix displacement $s(x, y)$ of all the lines projected on the test object, the matrix T', which containing all the lines projected on the reference plane, was also calculated. The displacement $s(x, y)$ is obtained by the difference between the matrices T and T', using Eq. (5.16).

The 3D shape of the object with high pixel density, in units of pixels, is shown in Fig. 5.13 where the reconstruction of the reference plane is omitted in the figure. However, to obtain the 3D shape in units of length (millimeters), it is necessary to calculate through a calibration process, the parameters $m(x, y)$ and

$n(x, y)$ of Eq. (5.2). The results of the calibration process are shown in the next section.

Finally, it is important to mention that some broken lines were connected to each other by cubic spline interpolation [68] due to the fact that they presented discontinuous small and the variations in the height of the object were smooth.

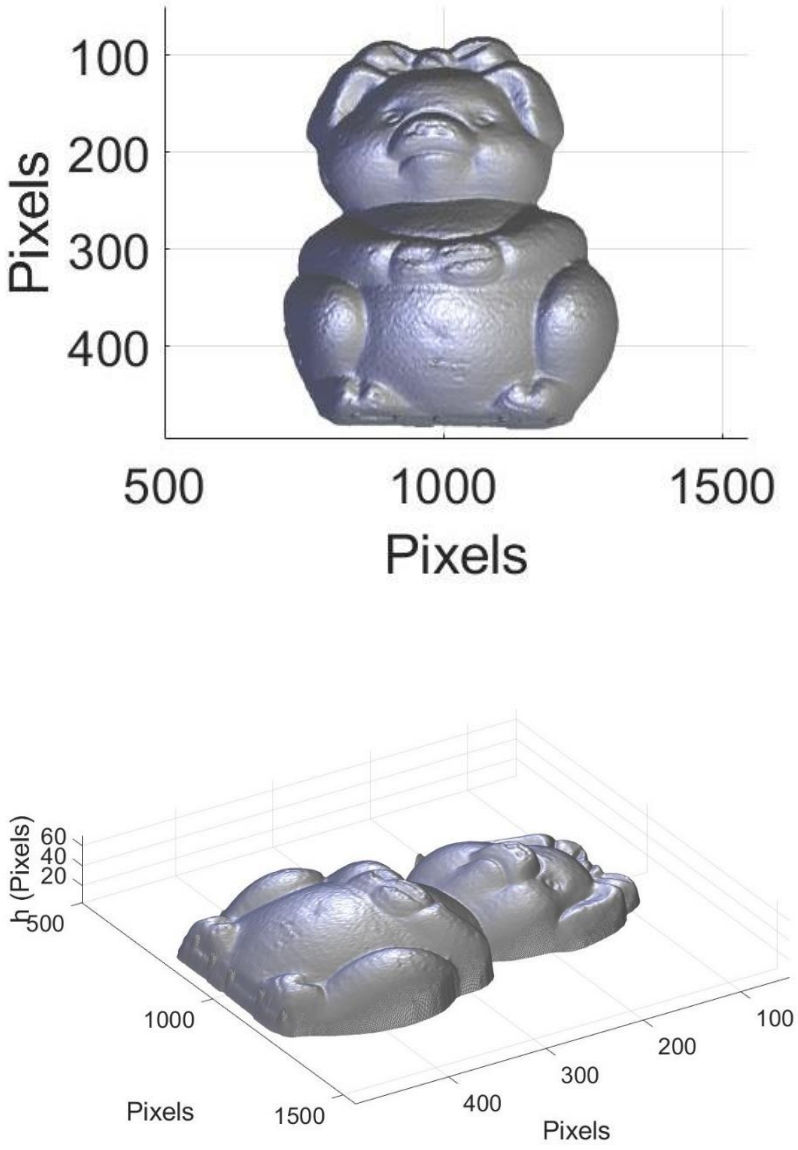

Figure 5.13. 3D shape of the test object with high pixel density at different viewing angles.

5.8.3 Results of obtaining three-dimensional measurements in real coordinates

The experimental scheme of Fig. 5.4 was set up to calibrate our 3D scanning system by color multi-line projection. A mechanical displacer moves the reference plane with a resolution of 2.5 μm at every step. The reference plane was moved towards the camera 25 positions of known heights h_i (where $i = 1, 2, \ldots, 25$), in 2 mm increments regarding an initial location ($z = 0$). In each position h_i, the skeleton positions of all the lines projected, represented by the matrix T were calculated with the same methodology used for the test object. Subsequently, the displacements $s(x, y)$ of the skeleton positions obtained in each position h_i, regarding the position $z = 0$, were determined. The values of $m(x, y)$ and $n(x, y)$ of each projected pixel of Eq. (5.2) were obtained by means of Eqs. (5.18) and (5.19), respectively. The values of $a_1(x, y)$, $a_2(x, y)$, $a_3(x, y)$, $b_1(x, y)$ and $b_2(x, y)$ of Eqs. (5.18) and (5.19) were calculated using the Eqs. (5.20), (5.21), (5.22), (5.23) and (5.24), respectively. Figs. 5.14.(a) and 5.14.(b) show a map with the distribution of values in each pixel of $m(x, y)$ and $n(x, y)$, respectively.

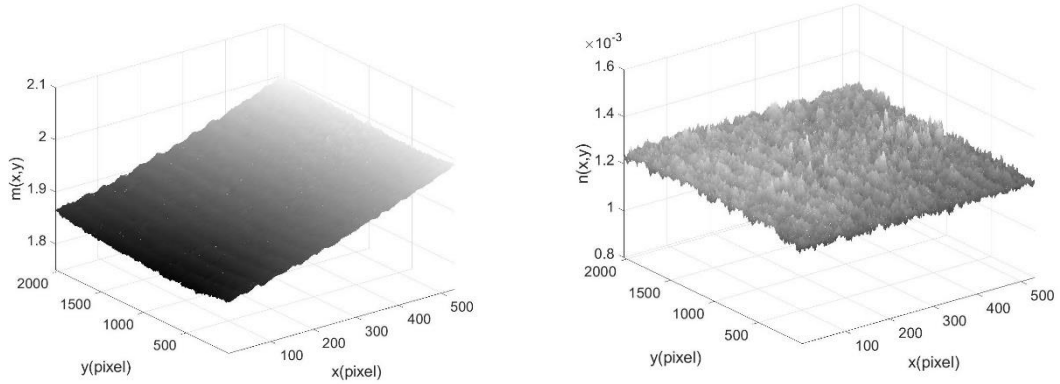

(a) (b)

Figure 5.14. (a) and **(b)** distribution of the $m(x, y)$ *and* $n(x, y)$ values obtained by the calibration process, respectively.

In Fig. 5.15.(a), the reference planes reconstructed by Eq. (5.17) are shown for the heights 10 mm, 20 mm, 30 mm, 40 mm and 50 mm, respectively. In Fig. 5.15.(b) the distribution of the RMS error values for each height value is shown. It is important to highlight the results of Fig. 5.15.(b), which shows that within the calibrated range of heights, in the worst case, our measurements will have an approximate RMS error of 0.055 mm, and an average RMS error of 0.02 mm. The results evidence the high accuracy obtained by our calibration proposal based on reference [10].

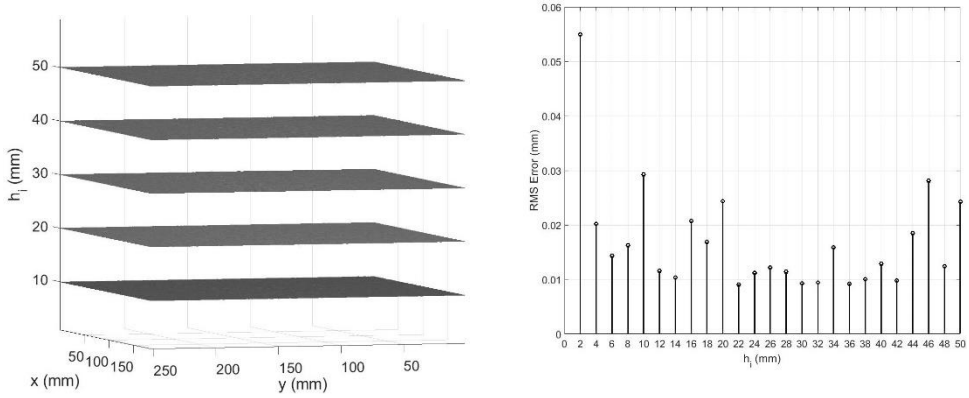

(a) (b)

Figure 5.15. (a) Reference planes reconstructed through the calibration process. **(b)** Distribution of the RMS error for each value of h_i.

Finally, after obtaining the distribution of values $m(x, y)$ and $n(x, y)$ for each pixel projected onto the reference plane, and also obtaining the displacements $s(x, y)$ of test object regarding the reference plane of all projected color lines, the 3D coordinates of the surface of the object in units of millimeters are obtained by Eq. (5.2). The result of the reconstructed test object in units of millimeters with high pixel density is shown in Fig. 5.16.

The efficiency of our proposal was also applied to other test objects shown in Figs. 5.17.(a) and 5.18.(a), where fine details of the surface of the objects were obtained. These good results with high pixel density are shown in the Figs. 5.17.(b) and 5.18.(b), respectively.

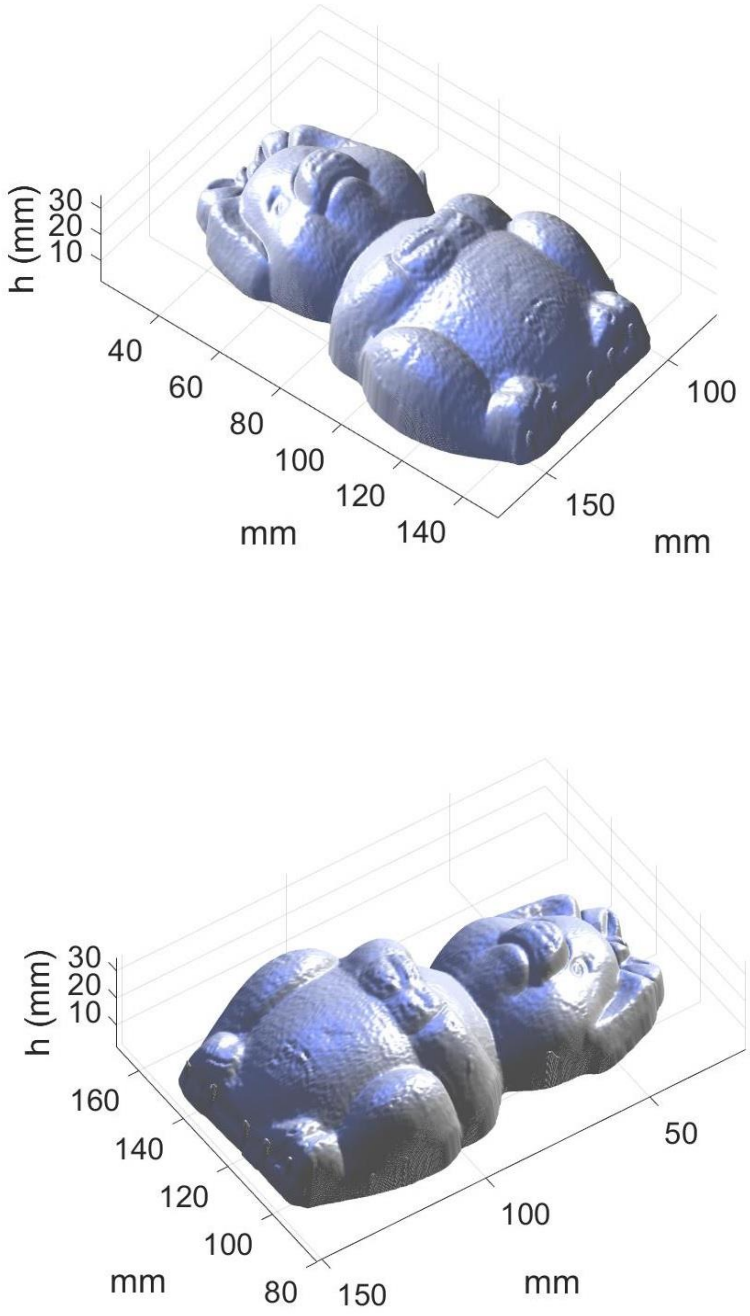

Figure 5.16. 3D shape of the object with high pixel density in units of millimeters at different viewing angles.

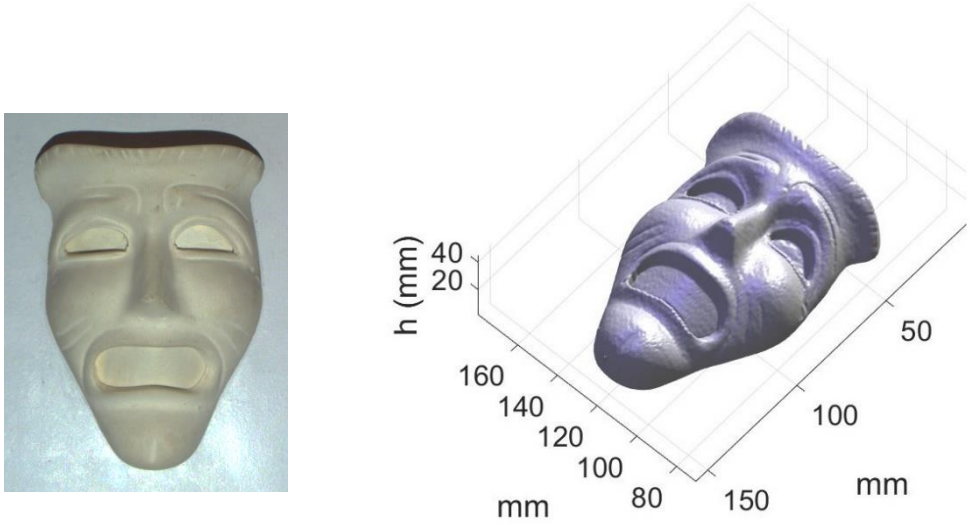

(a) (b)

Figure 5.17. (a) Second test object. **(b)** 3D scanning of the second under test.

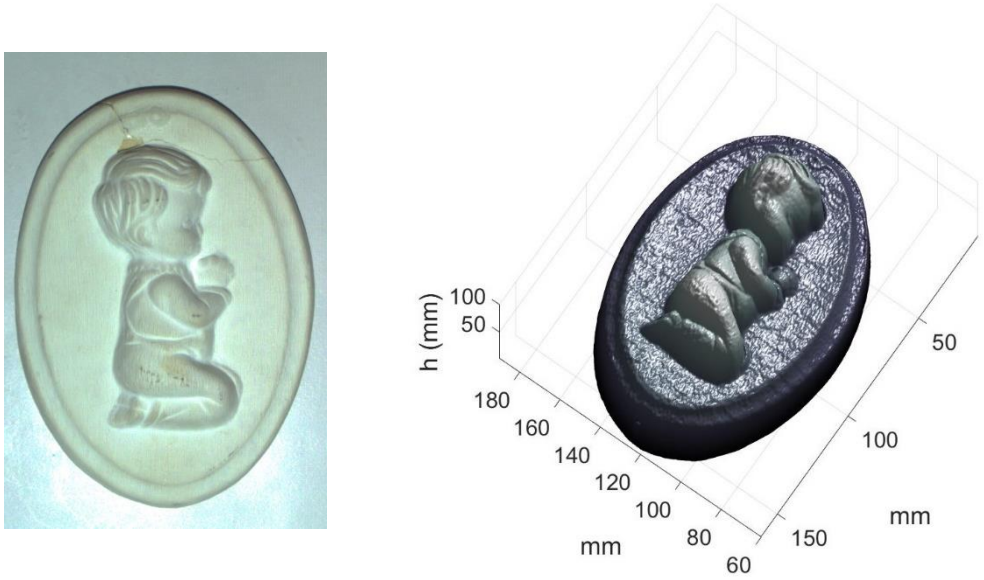

(a) (b)

Figure 5.18. (a) Third test object. **(b)** 3D scanning of the third under test.

5.9 CONCLUSIONS

In this chapter, 3D scanning of objects by the projection of a set of gratings with color structured multi-line was proposed. The proposal allows obtaining the 3D shape of objects with low-resolution by processing a single captured image of the gratings (see Fig. 5.12. (b)); results are comparable with references [25, 26, 31, 33]. In addition, by processing all the images captured from the gratings, the 3D shape of objects with high pixel density was obtained (see Figs. 5.16, 5.17 and 5.18), with the merit that the capture time of the images is 40 times faster compared to one light line projection technique [16]. This broadens the range of possibilities for future applications of techniques based on displacement of the light line.

The discontinuous light lines of the captured images were considerably reduced by using the morphological dilation operation. This significantly reduces the complexity of the grouping process of the line segments, which is a crucial step for the correct performance of our proposal.

Finally, three-dimensional measurements of objects were obtained in units of millimeters with errors less than 0.06 mm (see Fig 5.15. (b)) by means of a calibration method based on reference [10] which allows obtaining the distances between optical elements and each pixel projected on an object without the need to measure them directly.

CHAPTER 6: GENERAL CONCLUSIONS AND FUTURE WORKS

In this thesis, three types of 3D scanning methods of objects through calculating the displacement of the light lines by extraction of the skeleton were presented. Each proposed method allows us to give the following general conclusions.

Regarding 3D scanning by projection of white light profiles, the main contribution was to use the projection of three types of light profiles (Gaussian, triangular and sinusoidal), digitally generated by a multimedia projector, and to implement the respective algorithms to each profile to obtain the skeleton of the projected light line. The efficiency of the use of light profiles in 3D scanning of objects was quantitatively evaluated in terms of accuracy and processing time. Our results conclude the use of light projection with Gaussian profile to obtain more accuracy in the topography measurement, and the use of light with triangular profile to considerably improve the processing time and to obtain fast results. Depending on the application, in some situations accuracy or speed of measurements is required, therefore, the findings of the analysis of the white light profiles will allow us a better criterion to choose the most suitable profile to improve the performance of the technique and get convenient results on any application in question. It is important to highlight the use of the projector as a light source, instead of the traditional use of laser, since it avoids speckle noise, that is one of the most important factors that deteriorate the images of the light line and has an unfavorable influence on obtaining the skeleton and subsequently on the accuracy of the measurements.

Extending the study of the previous proposal, we proposed 3D scanning of object by projection of three color lines with Gaussian profile. The contribution of this proposal is that it allows simultaneous scanning in different areas of the object under study, optimizing in this way the number of images and the capture time compared to the projection of one light line. It is important to mention that to carry out this study, the color channels (red, green, and blue) were taken advantage of and were implemented segmentation algorithms by color which do not require threshold values, are robust to the color and reflectance of the object's surface, and ambient lighting.

Finally, based on the findings of previous studies, we propose 3D scanning of objects by color structured multi-line projection with gaussian profile. The main contribution of this proposal is to obtain the 3D shape of objects with high pixel density and precision,

with the merit that the image capture time is 40 times faster compared to the projection technique of one light line since only 14 images were necessary to process. The time for capturing the images through our scanning system was 0.47 s, which allows expanding the possibilities of future applications of this technique in the scanning of objects in motion or whose shape is variable over time. Other valuable contributions of this study were the proposal of a calibration method which allowed us to reach an RMS error of 0.055 mm in the measurements of the object heights; in addition, algorithms were implemented to reduce the number of broken lines, which allows the grouping process of the proposed light lines to be simpler and more efficient. Finally, it is important to mention that it was not necessary to implement complex phase unwrapping algorithms and the displacement of the light line was measured directly by skeletonization.

The criteria for choosing the proposals given in this thesis for scanning objects will depend on the complexity of the surface of the object and the requirements of the application, in case a high precision or speed of measurement is needed in the scanning.

The following future works are proposed:

Using a multimedia projector as a light source allows controlling the intensity of each projected pixel (impossible to control with laser light projection), that is why we propose the development of new methods that allow controlling the intensity of the projected light line based on the local reflectivity of the object's surface with the purpose of improving the contrast of light lines and greatly reducing discontinuities caused by low illumination in some areas of the surface. This study will increase the performance of object scanning.

The good results obtained in the scanning of objects were due to the fact that the skeletonization of the light lines was done through the use of Bezier polynomials of order 11; however, the order of the polynomial can lead to an overestimation or underestimation of the points that are fitted to the function. Therefore, we propose to develop algorithms where the order of the Bezier polynomials can be adaptive which may decrease unnecessary computational time for relatively smooth objects.

To apply the algorithms of structured light projection with triangular profile in the multi-line color scanning to increase the efficiency of the images processing time.

Increase the geometric versatility of the proposed scanning systems by calibrating the camera-projector pair. The points of correspondence between the projected pixels and

the pixels of the captured images will be obtained directly by the displacement of the light lines. Knowing the correspondence points, the object coordinates in three-dimensional space will be a function of the intrinsic and extrinsic parameters of the camera and the projector. This proposal will be based on the references [81, 82].

REFERENCES

1. Takeda, M. and K. Mutoh, *Fourier transform profilometry for the automatic measurement of 3-D object shapes.* Applied Optics, 1983. **22**(24): p. 3977-3982.
2. Takeda, M., H. Ina, and S. Kobayashi, *Fourier-transform method of fringe-pattern analysis for computer-based topography and interferometry.* JOSA, 1982. **72**(1): p. 156-160.
3. Takeda, M., *Fourier fringe analysis and its application to metrology of extreme physical phenomena: a review.* Applied Optics, 2013. **52**(1): p. 20-29.
4. Su, X. and W. Chen, *Fourier transform profilometry:: a review.* Optics and Lasers in Engineering, 2001. **35**(5): p. 263-284.
5. Zappa, E. and G. Busca, *Static and dynamic features of Fourier transform profilometry: A review.* Optics and Lasers in Engineering, 2012. **50**(8): p. 1140-1151.
6. Juarez-Salazar, R., et al., *How do phase-shifting algorithms work?* European Journal of Physics, 2018. **39**(6): p. 065302.
7. Zuo, C., et al., *Phase shifting algorithms for fringe projection profilometry: A review.* Optics and Lasers in Engineering, 2018. **109**: p. 23-59.
8. Servin, M., J. Estrada, and J.A. Quiroga, *The general theory of phase shifting algorithms.* Optics Express, 2009. **17**(24): p. 21867-21881.
9. Wang, Z., D.A. Nguyen, and J.C. Barnes, *Some practical considerations in fringe projection profilometry.* Optics and Lasers in Engineering, 2010. **48**(2): p. 218-225.
10. Jia, P., J. Kofman, and C.E. English, *Comparison of linear and nonlinear calibration methods for phase-measuring profilometry.* Optical Engineering, 2007. **46**(4): p. 043601.
11. Zhang, S., *Composite phase-shifting algorithm for absolute phase measurement.* Optics and Lasers in Engineering, 2012. **50**(11): p. 1538-1541.
12. Wang, F., et al., *Nonlinear control of a piezoelectric actuator system for a phase shift interferometer*. Journal of Optical Technology, 2019. **86**(5): p. 296-300.
13. González-Laprea, J., J. Cappelletto, and R. Escalona, *Frequency to voltage converter as a phase controller in phase shifting interference microscopy*. International Journal of Optomechatronics, 2011. **5**(1): p. 68-79.

14. Muñoz-Rodríguez, J.A. and R. Rodríguez-Vera, *Evaluation of the light line displacement location for object shape detection.* Journal of Modern Optics, 2003. **50**(1): p. 137-154.
15. Xu, X., et al., *Line structured light calibration method and centerline extraction: A review.* Results in Physics, 2020. **19**: p. 103637.
16. Vilchez-Rojas, H.L., J.A. Rayas, and A. Martínez-García, *Use of white light profiles for the contouring of objects.* Optics and Lasers in Engineering, 2020. **134**: p. 106295.
17. O'Leary, P. and M. Harker, *Surface modelling using discrete basis functions for real-time automatic inspection*, in *3-D Surface Geometry and Reconstruction: Developing Concepts and Applications*. 2012, IGI Global. p. 216-264.
18. Zhang, Y., et al., *Accuracy improvement in laser stripe extraction for large-scale triangulation scanning measurement system.* Optical Engineering, 2015. **54**(10): p. 105108.
19. Usamentiaga, R., J. Molleda, and D.F. García, *Fast and robust laser stripe extraction for 3D reconstruction in industrial environments.* Machine Vision and Applications, 2012. **23**(1): p. 179-196.
20. Villán, A.F., et al., *Low-cost system for weld tracking based on artificial vision.* IEEE Transactions on Industry Applications, 2011. **47**(3): p. 1159-1167.
21. Yuehua, L., et al. *An improved gray weighted method for sub-pixel center extraction of structured light stripe*. in *2016 10th International Conference on Sensing Technology*. 2016. IEEE.
22. Amir, Y.M. and B. Thörnberg, *High precision laser scanning of metallic surfaces.* International Journal of Optics, 2017. **2017**.
23. Zhixin, H., et al., *Adaptive centre extraction method for structured light stripes.* Ukrainian Journal of Physical Optics, 2017(18,№ 1): p. 9-19.
24. Qingguo, T., et al., *Utilizing polygon segmentation technique to extract and optimize light stripe centerline in line-structured laser 3D scanner.* Pattern Recognition, 2016. **55**: p. 100-113.
25. Wang, Z., *Robust three-dimensional face reconstruction by one-shot structured light line pattern.* Optics and Lasers in Engineering, 2020. **124**: p. 105798.
26. Wang, Z. and Y. Yang, *Single-shot three-dimensional reconstruction based on structured light line pattern.* Optics and Lasers in Engineering, 2018. **106**: p. 10-16.

27. Willomitzer, F. and G. Häusler, *Single-shot 3D motion picture camera with a dense point cloud.* Optics Express, 2017. **25**(19): p. 23451-23464.
28. Willomitzer, F., et al., *Single-shot three-dimensional sensing with improved data density.* Applied Optics, 2015. **54**(3): p. 408-417.
29. Willomitzer, F., et al. *Flying Triangulation-a motion-robust optical 3D sensor for the real-time shape acquisition of complex objects*. in *AIP Conference Proceedings*. 2013. American Institute of Physics.
30. Willomitzer, F., *Single-Shot 3D Sensing Close to Physical Limits and Information Limits*. 2019: Springer.
31. Li, W., et al., *3D measurement system based on divergent multi-line structured light projection, its accuracy analysis.* Optik, 2021. **231**: p. 166396.
32. Willomitzer, F., et al., *Flying Triangulation–towards the 3D movie camera*, in *Fringe 2013*. 2014, Springer. p. 895-898.
33. Li, W., et al., *Multi-line laser projection 3D measurement simulation system technology.* Optik, 2021. **231**: p. 166390.
34. Tornslev, K., *3D scanning using multibeam laser*. 2005: Informatik og Matematisk Modellering, Danmarks Tekniske Universitet.
35. Pajares Martinsanz, G., C. García, and M. Jesús, *Visión por computador: imágenes digitales y aplicaciones*. 2002.
36. Raid, A., et al., *Image restoration based on morphological operations.* International Journal of Computer Science, Engineering and Information Technology (IJCSEIT), 2014. **4**(3): p. 9-21.
37. Koller, D. and M. Levoy, *Protecting 3d graphics content.* Communications of the ACM, 2005. **48**(6): p. 74-80.
38. Huang, W. and R. Kovacevic, *A laser-based vision system for weld quality inspection.* Sensors, 2011. **11**(1): p. 506-521.
39. Schlarp, J., E. Csencsics, and G. Schitter, *Optical scanning of laser line sensors for 3D imaging.* Applied Optics, 2018. **57**(18): p. 5242-5248.
40. Geng, Z. and B. Bidanda, *Review of reverse engineering systems–current state of the art.* Virtual and Physical Prototyping, 2017. **12**(2): p. 161-172.
41. Shanoer, M.M. and F.M. Abed, *Evaluate 3D laser point clouds registration for cultural heritage documentation.* The Egyptian Journal of Remote Sensing and Space Science, 2018. **21**(3): p. 295-304.

42. Wu, J., Y. Li, and Y. Zhang, *Use of intraoral scanning and 3-dimensional printing in the fabrication of a removable partial denture for a patient with limited mouth opening.* The Journal of the American Dental Association, 2017. **148**(5): p. 338-341.
43. Kato, J.-I., *Fringe analysis*, in *Handbook of Optical Metrology*. 2017, CRC Press. p. 541-553.
44. Zhang, S., *Absolute phase retrieval methods for digital fringe projection profilometry: A review.* Optics and Lasers in Engineering, 2018. **107**: p. 28-37.
45. Ghiglia, D.C., *Two-Dimentional Phase Unwrapping: Theory*. Algorithms, and Software, 1998.
46. Abdul-Rahman, H.S., et al., *Fast and robust three-dimensional best path phase unwrapping algorithm.* Applied Optics, 2007. **46**(26): p. 6623-6635.
47. Rayas, J., et al. *Gates' interferometer as fringe projection system for recovering 3D shapes*. in *Emerging Challenges for Experimental Mechanics in Energy and Environmental Applications, Proceedings of the 5th International Symposium on Experimental Mechanics and 9th Symposium on Optics in Industry (ISEM-SOI), 2015*. 2017. Springer.
48. Martínez, A., et al., *Leaf cuticle topography retrieved by using fringe projection.* Optics and Lasers in Engineering, 2012. **50**(2): p. 231-235.
49. Pan, B., et al., *Phase error analysis and compensation for nonsinusoidal waveforms in phase-shifting digital fringe projection profilometry*. Optics Letters, 2009. **34**(4): p. 416-418.
50. Guo, H., H. He, and M. Chen, *Gamma correction for digital fringe projection profilometry.* Applied Optics, 2004. **43**(14): p. 2906-2914.
51. Ye, X., et al., *Gamma correction for three-dimensional object measurement by phase measuring profilometry.* Optik, 2015. **126**(24): p. 5534-5538.
52. Sert, E., I.T. Okumus, and D. Taskin, *3D Modelling with Structured Light Gamma Calibration.* Advances in Electrical and Electronic Engineering, 2014. **12**(4): p. 347-353.
53. García, A.M., et al. *Iterative estimation of the topography by means of structured light*. in *Optical Inspection and Metrology for Non-Optics Industries*. 2009. International Society for Optics and Photonics.
54. Martínez, A., et al., *Iterative estimation of the topography measurement by fringe-projection method with divergent illumination by considering the pitch variation*

along the x and z directions. Optics and Lasers in Engineering, 2010. **48**(9): p. 877-881.

55. Gåsvik, K.J., K.G. Robbersmyr, and T. Vadseth, *Projected fringes for the measurement of large aluminum ingots.* Measurement Science and Technology, 2010. **21**(10): p. 105302.
56. Gåsvik, K.J., et al., *Deformation measurement of circular steel plates using projected fringes.* The International Journal of Advanced Manufacturing Technology, 2014. **70**(1): p. 321-326.
57. Willomitzer, F., et al. *Detection and correction of line indexing ambiguities in Flying Triangulation*. in *Proceedings of the 114th DGaO Conference, A12*. 2013.
58. Naidu, D. and R.B. Fisher, *A comparative analysis of algorithms for determining the peak position of a stripe to sub-pixel accuracy*, in *BMVC91*. 1991, Springer. p. 217-225.
59. Munoz-Rodriguez, J.A., R. Rodriguez-Vera, and M. Servin, *Direct object shape detection based on skeleton extraction of a light line.* Optical Engineering, 2000. **39**.
60. Li, Y., et al., *Sub-pixel extraction of laser stripe center using an improved gray-gravity method.* Sensors, 2017. **17**(4): p. 814.
61. Wu, X., et al., *A novel high precise laser 3D profile scanning method with flexible calibration.* Optics and Lasers in Engineering, 2020. **132**: p. 105938.
62. Jun, W., et al. *Extraction of centerline of large-format laser stripes against ambient light interference*. in *Journal of Physics: Conference Series*. 2021. IOP Publishing.
63. Wang, Z. and C. Zhang, *Three-dimensional hand reconstruction by single-shot structured light line pattern.* IEEE Access, 2018. **6**: p. 59881-59890.
64. Jecić, S. and N. Drvar. *The assessment of structured light and laser scanning methods in 3D shape measurements*. in *Proceedings of the 4th International Congress of Croatian Society of Mechanics*. 2003. Citeseer.
65. Sun, Q., J. Chen, and C. Li, *A robust method to extract a laser stripe centre based on grey level moment.* Optics and Lasers in Engineering, 2015. **67**: p. 122-127.
66. Lv, Z. and Z. Zhang, *Build 3D Scanner System based on Binocular Stereo Vision.* Journal of Computers, 2012. **7**(2): p. 702399404.
67. Dong, Z., et al., *Measurement of free-form curved surfaces using laser triangulation.* Sensors, 2018. **18**(10): p. 3527.

68. Munoz-Rodriguez, J.A., R. Rodriguez-Vera, and M.S. Guirado, *Direct object shape detection based on skeleton extraction of a light line.* Optical Engineering, 2000. **39**(9): p. 2463-2471.
69. Press, W.H., et al., *Numerical recipes 3rd edition: The art of scientific computing*. 2007: Cambridge University Press.
70. da Silva Brum, R., et al., *A Matlab code to fit periodic data.* Revista Brasileira de Computação Aplicada, 2015. **7**(2): p. 16-25.
71. Je, C., *Color structured light for rapid range imaging*. 2008, Sogang University, Seoul, Korea.
72. Zhang, Z., *Review of single-shot 3D shape measurement by phase calculation-based fringe projection techniques.* Optics and Lasers in Engineering, 2012. **50**(8): p. 1097-1106.
73. Lin, H., L. Nie, and Z. Song, *A single-shot structured light means by encoding both color and geometrical features.* Pattern Recognition, 2016. **54**: p. 178-189.
74. Nikolaev, D.P. and P.P. Nikolayev, *Linear color segmentation and its implementation.* Computer Vision and Image Understanding, 2004. **94**(1-3): p. 115-139.
75. Fechteler, P. and P. Eisert, *Adaptive colour classification for structured light systems.* IET Computer Vision, 2009. **3**(2): p. 49-59.
76. Fechteler, P., P. Eisert, and J. Rurainsky. *Fast and high resolution 3D face scanning*. in *2007 IEEE International Conference on Image Processing*. 2007. IEEE.
77. Je, C., K.H. Lee, and S.W. Lee, *Multi-projector color structured-light vision.* Signal Processing: Image Communication, 2013. **28**(9): p. 1046-1058.
78. Sreedhar, K. and B. Panlal, *Enhancement of images using morphological transformation.* International Journal of Computer Science & Information Technology, 2012. **4**(1).
79. Muñoz-Rodríguez, J.A., *Shape connection by pattern recognition and laser metrology.* Applied Optics, 2008. **47**(20): p. 3590-3608.
80. Haralick, R.M. and L.G. Shapiro, *Connected components labeling.* Computer and Robot Vision, 1992. **1**: p. 28-48.
81. Juarez-Salazar, R. and V.H. Diaz-Ramirez, *Flexible camera-projector calibration using superposed color checkerboards.* Optics and Lasers in Engineering, 2019. **120**: p. 59-65.

82. Juarez-Salazar, R., et al., *Key concepts for phase-to-coordinate conversion in fringe projection systems.* Applied Optics, 2019. **58**(18): p. 4828-4834.

ANNEXED

Publication

Vilchez-Rojas, H.L., J.A. Rayas, and A. Martínez-García, *Use of white light profiles for the contouring of objects.* Optics and Lasers in Engineering, 2020. **134**: p. 106295.

Publications under review

Vilchez-Rojas, H.L., A. Martínez-García, and J.A. Rayas, *3D scanning of objects by projection of three incoherent RGB lines with Gaussian profile*.

Vilchez-Rojas, H.L., J.A. Rayas, and A. Martínez-García, *3D scanning of objects by color multi-line structured light projection.*

Congress

The Iberoamerican Optics Meeting and the Latinamerican Meeting on Optics, Lasers and Applications (RIAO-OPTILAS), *Proyección de una línea de luz usando un proyector multimedia para la reconstrucción 3D de objetos*, H. Vilchez-Rojas, A. Martínez-García, Juan A. Rayas, Cancún, México, September 2019.